Mars' Water Cycle and Escape: A View from Mars Express and Beyond

Franck Montmessin, A Fedorova, J Alday, S Aoki, M Chaffin, Jean-Yves Chaufray, T Encrenaz, T Fouchet, Elise Wright Knutsen, O Korablev, et al.

Space Science Reviews (2024) 220:77
https://doi.org/10.1007/s11214-024-01099-6

Mars' Water Cycle and Escape: A View from Mars Express and Beyond

F. Montmessin[1] · A. Fedorova[2] · J. Alday[3] · S. Aoki[4] · M. Chaffin[5] · J.-Y. Chaufray[1] · T. Encrenaz[6] · T. Fouchet[6] · E.W. Knutsen[1] · O. Korablev[2] · G. Liuzzi[7,8] · M.A. Mayyasi[9] · A. Pankine[10] · A. Trokhimovskiy[2] · G.L. Villanueva[8]

Received: 14 August 2023 / Accepted: 1 August 2024

Abstract
The search for water on Mars has long been a theme of intense exploration, as it represents a means of addressing Mars' current climate as well as its evolution in the recent and more distant past. Since the 1970s, several missions have carried instruments to track water in the atmosphere, leading to the conceptualization of a water cycle on Mars characterized by intense seasonal variability in water vapor abundance across the planet. After Mariner 9, Viking, Phobos 2 and Mars Global Surveyor, Mars Express has become the fifth orbiter capable of detecting water vapour, with unique features: measurements by several instruments, each probing a distinct wavelength region from near-infrared to thermal infrared, altitude-dependent profiling of water thanks to solar occultation, and observation in the exosphere of its by-product, hydrogen atoms, which can escape into space, depriving Mars of its primordial water reservoir. Thanks to Mars Express, a new vision of Mars' water cycle and escape processes has emerged. The achievements of Mars Express, as well as the legacy of other missions, which established the foundations of our understanding of Mars' water cycle are presented in this article.

✉ F. Montmessin
franck.montmessin@latmos.ispl.fr

1 Laboratoire Atmosphères, Observations Spatiales, CNRS, Guyancourt, France

2 Space Science Institute, Moscow, Russia

3 Open University, Milton Keynes, UK

4 Department of Complexity Science and Engineering, Graduate School of Frontier Sciences, The University of Tokyo, Kashiwa, Japan

5 Laboratory for Atmospheric and Space Physics, Boulder, CO, USA

6 Laboratoire d'Études Spatiales et d'Instrumentation en Astrophysique, Observatoire de Paris-PSL, CNRS, Sorbonne Université, Université de Paris Cité, Meudon, France

7 Department of Physics, American University, Washington, DC, USA

8 NASA Goddard Space Flight Center, Greenbelt, MD, USA

9 Boston University, Boston, MA, USA

10 Space Science Institute, Boulder, CO, USA

Published online: 30 September 2024

Keywords Mars · Atmosphere · Water cycle · Mars Express · Mars Orbiters · Hydrogen · Escape

1 Introduction

1.1 Mars' Water Cycle... Before Mars Express

Before Mars Express (henceforth MEx), what we knew of water in the Martian atmosphere was mostly based on ground-based observations and two historical missions; Viking (near the end of the 70s) and Mars Global Surveyor (MGS, around the 2000s). These two missions have laid the foundation for what is now commonly referred to as the "Mars' water cycle". Although there is more to the water cycle than the sole behavior of water (either as vapor or clouds) in the atmosphere, the latter is the best "informant" of the exchanges between the atmosphere and (sub)surface reservoirs, which shape the observed seasonal variations of water.

Water vapor in the Martian atmosphere was first detected by Spinrad et al. (1963) from the weak 0.83 μm near-infrared (NIR) band of water using the Mount Wilson 100-inch refractor. Water vapor was also reported by the Mariner 9 orbiter in the thermal infrared (TIR) using the 30-μm rotational band (Conrath et al. 1973), showing prominent seasonal variations in its column abundance (expressed as precipitable μm or pr-μm which is equivalent to g/cm^{-2}) at both poles, with a maximum of 20-30 pr-μm observed above the North Polar Cap (NPC) in spring.

The first climatology of water vapor, encompassing more than one Martian year, was produced by the Martian Atmospheric Water Detectors (MAWD) on-board the two Viking Orbiters using the 1.38 μm absorption water band (Jakosky and Farmer 1982; see Fig. 1). This climatology has become a "classic" of Mars' exploration, for it revealed the essential role of the NPC in pacing the water cycle. Once exposed to the Sun in springtime, the NPC was observed to release the equivalent of ∼1 km^3 of ice. This episode of sublimation produced the highest water vapor abundance of the year, with as much as 100 pr-μm spreading gradually away from the north polar region to pool in the tropics and then move to the other hemisphere. Interestingly, a 15 pr-μm peak was also observed around the South Pole in southern summer, where no perennial water ice had ever been observed, the only perennial ice known at the surface being made of CO_2. This asymmetry of water abundances between the two hemispheres led Jakosky and Farmer (1982) to speculate about the existence of a North-to-South net flow of water on an annual basis, thereby questioning the long-term stability of the NPC.

A new intensive orbital survey began at the end of the 1990s with Mars Global Surveyor (MGS). The Thermal Emission Spectrometer (TES) monitored the spatial and seasonal dependence of temperature structure, dust, water vapor and ice clouds, for three consecutive Martian years between 1997 and 2004 (Smith 2004). These data led to dividing Mars's climate into two main periods: 1) the warm, dusty, and strongly variable perihelion season ($L_s = 180°$-$360°$) that is now known to host the stochastic Global Dust Events, and 2) the cool, dust-free, cloudy, and stable aphelion season ($L_s = 0°$-$180°$). Regarding water, peak abundances were observed near the two poles, respectively ∼100 pr-μm in the North and ∼50 pr-μm in the South (Smith 2002), in line with MAWD data. TES data imply some cross-equatorial transport of water from the North to the South during northern summer, uncompensated by a corresponding flow to the North in the opposite season. This transport could be significantly disrupted by large dust storms, combined with the fact that peak vapor

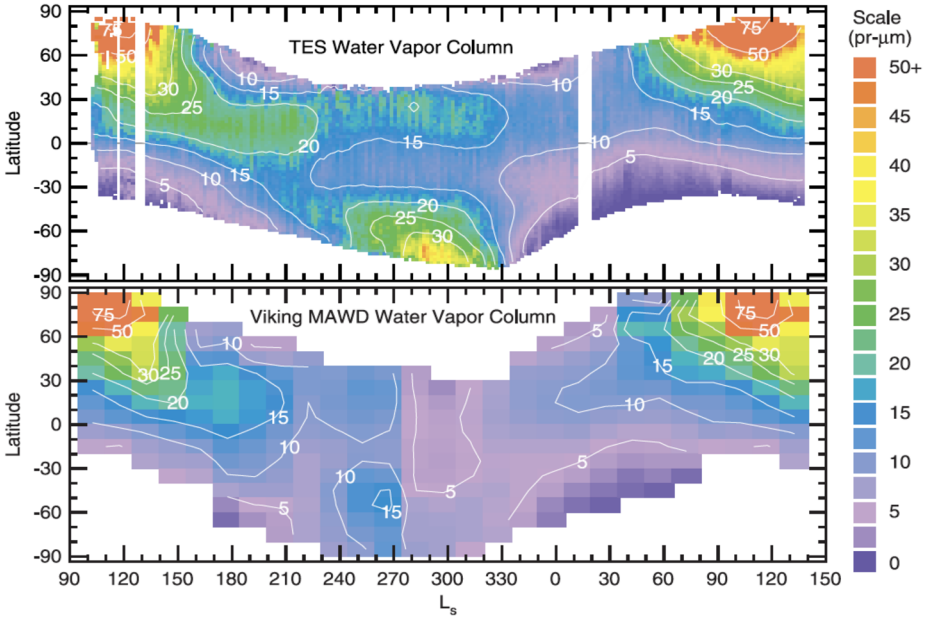

Fig. 1 The seasonal and latitudinal evolution of water column abundances as observed (top) by MGS/TES in the TIR and (bottom) by Viking/MAWD instrument in the NIR (Jakosky and Farmer 1982). The two exhibit the same major features of the water cycle, with northern summer peaks above the NPC that seem to then slowly humidify the rest of the Martian atmosphere. From Smith (2002). Reprinted with permission from Wiley

abundances are significantly reduced in the South, when large-to-global dust storms occur (Pankine and Tamppari 2019; Pankine et al. 2023).

TES and MAWD observations reveal a similar seasonal cycle but also show some differences, especially at the summer pole in the South where TES reports three times more water than MAWD. This difference has been attributed to the high dust opacity that usually prevails in southern summer and that impaired the retrievals of Jakosky and Farmer (1982) who neglected the effect of multiple scattering. This disagreement was almost entirely explained by the reanalysis of Fedorova et al. (2004) who demonstrated the importance of multiple-scattering for near-IR retrievals of water vapor (see Sect. 5).

1.2 The View from Theory

Although incomplete, with its vertical distribution barely explored, the numerous enigmas posed by the MAWD and TES Mars water vapor datasets have been pivotal in paving the way for an active modeling era marked by the introduction of 3D climate models of Mars (Richardson and Wilson 2002a; Montmessin et al. 2004). These models, building on the pioneering effort of Houben et al. (1997), allowed identifying several key mechanisms responsible for maintaining Mars' water cycle in a steady-state, with perhaps a small net annual flux towards the South (confirming the early speculations of Jakosky and Farmer 1982). These mechanisms rely on an efficient horizontal mixing of the atmosphere (that is Mars' weather) that regulates the polar extraction and return of water, by reducing the equator-to-pole gradient of water vapor all year long. Moreover, the North and South hemispheres communicate via the single solstitial global circulation cell, which changes orientation between aphelion

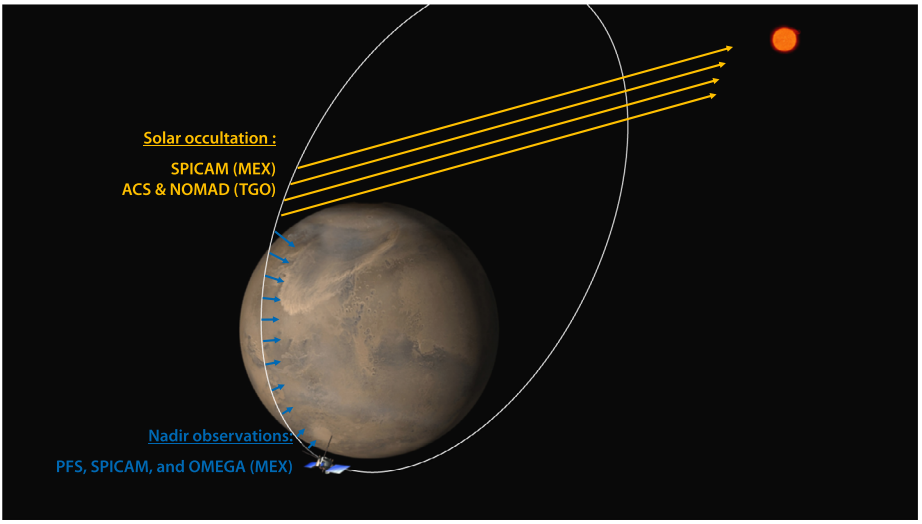

Fig. 2 Sketch showing the way observations have been done by MEx, to measure water vapor column abundance (nadir) or water vapor profiles (solar occultation)

and perihelion seasons. The way this cell operates and combines with the colder aphelion climate promotes water retention in the North on an annual basis (Clancy et al. 1996).

1.3 Mars Express "Delivers"...

At the beginning of MEx, the main features of the water vapor horizontal distribution, which still form the classical picture of its seasonal cycle, were already known from previous missions and measurements. Yet, a knowledge gap remained regarding its vertical distribution. The first observations of the vertical distribution of water vapor were derived from the Auguste solar occultation experiment on-board Phobos 2, which operated two months after its arrival at Mars in 1989, producing only a handful of profiles. These observations revealed a sharp decrease in water vapor mixing ratio above 25 km, and a quasi-constant mixing ratio of ~100 ppmv below 20 km (Rodin et al. 1997). These early results revealed the Martian hygropause, above which water vapor is expected to decline due to the colder atmosphere that imposes lower vapor pressure and subsequent water ice cloud formation. While the database of water vapor profiles also comprised ground-based measurements (Clancy et al. 1996), it was too restricted to meaningfully address the behavior of water with altitude and constrain the mechanisms that control its journey in the atmosphere; a gap that MEx subsequently filled thanks to the regular use of solar occultation campaigns.

For the first time in Mars exploration, a mission was equipped (see an illustration of its main operating modes in Fig. 2) to comprehensively and redundantly explore present-day Mars water in all its forms; from the perennial ice at the poles, to the mid-to-high latitude frost that forms and vanishes every season, to water vapor and clouds which travel across the Martian globe enabling distant surface reservoirs to exchange on short timescales, as well as water adsorbed in the regolith.

Since Mars has apparently lost most of its water (Carr 1987), the question of its fate can also be considered from an atmospheric perspective. This is also a topic to which MEx has made major contributions. With its capacity to probe Lyman-α emission that originates

from the outer fringes of the Martian atmosphere, MEx was also capable of sensing the link between water and its by-product, namely hydrogen atoms. Their fate in the exosphere, as a light species, is tied to escape to space, making Mars leak its primordial water (indirectly) throughout ages. Together with the Trace Gas Orbiter (TGO) and the MAVEN missions, a new paradigm has emerged from the pioneering survey of the Martian exosphere accomplished by MEx, illuminating the path of Martian water to space.

The aim of this article is to present the main results that MEx has been able to accumulate after 20 years of exploring present-day water on Mars. Over this long period, MEx has been able both to confirm, extend and improve the results of previous missions using similar techniques, and at the same time to open up new perspectives employing new types observations. The text has placed its many discoveries in the rich context of all the other missions, focusing on those that have explored in much greater detail the new avenues opened up by MEx, in particular the characterisation of the vertical structure of water and the link between water in the lower atmosphere and escape. We are paying particular attention to the ExoMars Trace Gas Orbiter mission, which has perpetuated and extended the exploration of the Martian atmosphere by MEx. Together with MEx, all these missions have contributed to making the water cycle on Mars an increasingly familiar object of active research.

2 Observing Water in the Atmosphere and on the Ground with Mars Express

For additional information on the MEx instruments used to conduct water vapor measurements, the reader is referred to Wilson et al. (2024, this collection).

2.1 The Planetary Fourier Spectrometer (PFS)

PFS is a double-channel Fourier-transform spectrometer optimized for primarily atmospheric measurements (Formisano et al. 2005). The spectral range covered was from the near-IR (1.2–5.5 μm) in a short wavelength (SW) channel to thermal IR (5.5–45 μm) in a long-wavelength (LW) channel. Both channels feature a spectral resolution of 1.3–1.4 cm^{-1}. The spectrometer operates mostly in nadir geometry, with occasional pointing to selected areas or limb observations. With a Field Of View (FOV) of ∼2.8° and a spectrum acquisition time of 4 s, PFS offers a resolution of 12–30 km, while different forms of binning were usually applied to improve the signal-to-noise ratio. To measure water vapor abundance in nadir, PFS spectra were processed both in the near-IR, using the strongest 2.56-μm band (Tschimmel et al. 2008) and in the thermal-IR, where it captures the major part of the extended 30-μm water vapor band (Fouchet et al. 2007; see Fig. 3-top).

2.2 The SPectroscopy for Investigation of Characteristics of the Atmosphere of Mars (SPICAM) IR Spectrometer

SPICAM IR channel operates in the near-IR from 1 to 1.7 μm with a resolving power $\lambda/\Delta\lambda$ of ∼2000 (3.5-4 cm^{-1}) as described in Bertaux et al. (2006) and Korablev et al. (2006). The spectrometer possesses two optical entries to accommodate a large range of source brightness; one to look at Mars (nadir, limb), the other to look at the Sun when performing solar occultation. SPICAM measures water vapor abundance at 1.38 μm (see Fig. 3-middle), like MAWD on Viking 1 and 2. With an FOV of ∼1° and a spectrum acquisition time of 2.4 s, SPICAM IR has a nadir footprint of ∼30 km on the surface.

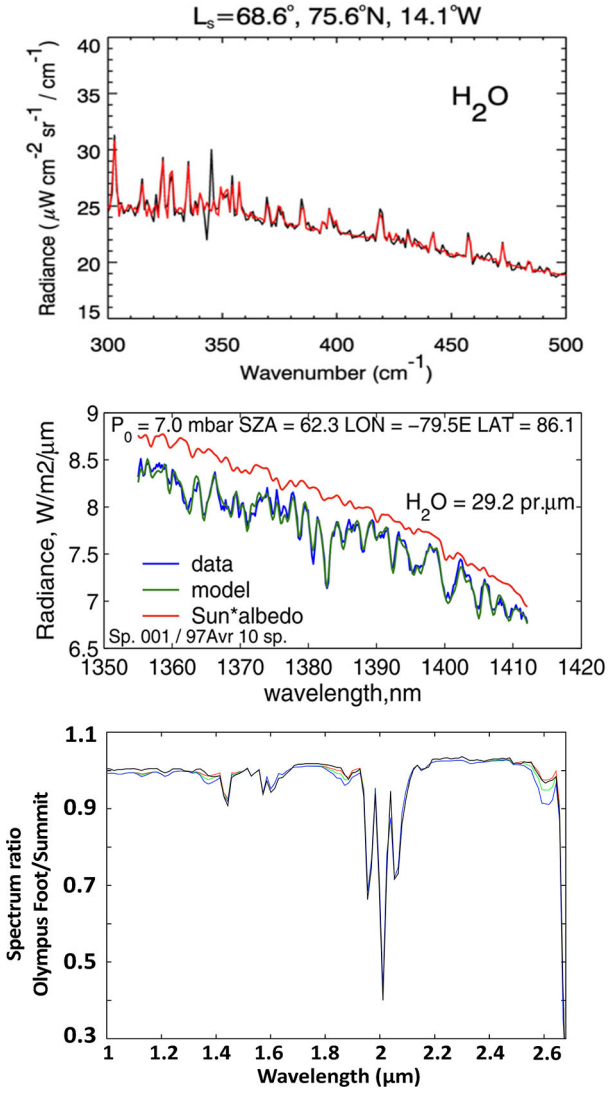

Fig. 3 Examples of spectra collected by (top) PFS (black: data, red: model) from Fouchet et al. (2007), (middle) SPICAM IR from Fedorova et al. (2006), and (bottom) OMEGA from Encrenaz et al. (2005). OMEGA spectra are given as ratios of raw spectra, with the denominator being the spectrum taken at the summit of Olympus Mons. Only the black curve is an actual observation; the other colors correspond to synthetic spectra with varying amounts of water vapor, the best fit being obtained with 150 ppmv. Reproduced with permission; copyright by (top) Elsevier, (middle) AGU, (bottom) ESO

2.2.1 Nadir Mode

As alluded to above, the retrieval of water vapor in the near-IR is sensitive to multiple scattering caused by dust and/or clouds (Fedorova et al. 2004). Fedorova et al. (2006), in the first SPICAM survey of water vapor, estimated the effect of dust to be marginal for air mass factor <3.5, and thus published data limited to an air mass factor <4. Clouds were identified to have a strong effect, and the water column-abundance was known to be biased low when probing cloudy areas, like the equatorial cloud belt during aphelion. Without concomitant estimations of dust or cloud opacity, Fedorova et al. (2006) could not include aerosol scattering and had to ignore dust or cloud effects. Yet, their work was an improvement over MAWD results extracted from the same spectral range, as they demonstrated the importance of using up-to-date spectroscopy (Sect. 5).

An extended and improved climatology was later presented by Trokhimovskiy et al. (2015, see Sect. 5), covering the 2004-2013 period, that is Martian Year 27 to 31.

A methodology introduced by Montmessin and Ferron (2019) was later employed by Knutsen et al. (2022) to not only measure the column abundance of water vapor, but also constrain its vertical distribution over nearly seven Martian Years (albeit with many data gaps). To achieve this, these authors have leveraged the unique MEx ability to measure water vapor in distinct spectral ranges. When combining simultaneous SPICAM near-IR (at 1.38 μm) and PFS thermal IR (at 20-35 μm) nadir observations, a synergistic spectrum can be created from two spectral ranges that have sensitivity to distinct portions of the atmospheric column. Retrieving water in this way places stronger constraints on how to adjust the vertical distribution of water vapor to fit observations. Typically, increased sensitivity to the fraction of water contained in the lowest 5 km of the column can be achieved while significantly reducing the uncertainty in the column abundance (see Sect. 6).

2.2.2 Occultation Mode

SPICAM IR is the only MEx instrument that can operate during solar occultations to profile the atmospheric composition. During an occultation sequence, every spectrum collected while staring at the Sun through the atmosphere is referenced by the bare Sun spectrum collected at the beginning (occultation) or the end (de-occultation) of the sequence. The vertical resolution depends on the distance of the spacecraft to the limb: the occultation instantaneous field-of-view (IFOV) of 4.2 arcmin (0.07°) yields 4-5 km on average, varying from 1 to 12 km. No observations could be made in MY 27 due to inadequate instrument commanding that disabled the acquisition of the CO_2 band domain, which allows deriving a mixing ratio for H_2O. The first retrievals and the method are presented in Fedorova et al. (2009), who analyzed 24 occultations collected during the northern spring of MY28. A typical profile measured by SPICAM IR delivers at every altitude H_2O (at 1.38 μm) and CO_2 (at 1.43 μm) concentrations (molecules.cm^{-3}), as well as the aerosol extinction (m^{-1}) extracted from the continuum. The profile encompasses the troposphere (from 5 to 30 km, depending on the dust loading that can fully obstruct the line-of-sight, henceforth LOS) to the upper mesosphere (up to 80 km when water is abundant at high altitude).

2.3 The "Observatoire pour La Minéralogie, l'Eau, les Glaces et l'Activité" hyperspectral imager (OMEGA)

The OMEGA NIR mapping spectrometer has been operating from 0.3 to 5.2 μm with a spectral sampling of 20 nm above 2.5 μm (corresponding to a spectral resolving power of 125 at 2.5 μm). Its IFOV of 1.2 mrad corresponds to about 300 m at the martian surface near periapsis. The cross track FOV (perpendicular to the spacecraft motion) varies from 16 to 128 × IFOV, depending on the operating mode of the observing sequence.

Although mainly designed to study mineralogical features at the surface of Mars, OMEGA was also able to monitor the water vapor content in the martian atmosphere. In particular, its high spatial resolution allowed mapping the sublimation phase of water above the ice caps (Encrenaz et al. 2005; Melchiorri et al. 2007, 2009) and the long-term monitoring enabled the study of seasonal variations (Encrenaz et al. 2008; Maltagliati et al. 2011). The strongest H_2O signature in the OMEGA spectral range was used, i.e., the (ν_1, ν_3) band of H_2O at 2.6 μm (Fig. 3-bottom). A spectrum recorded above Olympus Mons was selected as a reference, to eliminate the uncertainty associated with the OMEGA instrumental transfer function. The synthetic spectrum associated with the reference spectrum was calculated using the MOLA altimetry data and the Mars Climate Database for the atmospheric parameters.

2.4 Revisiting Water: The Advent of the Trace Gas Orbiter (TGO)

As its name suggests, TGO has been designed to measure trace components in the Martian atmosphere with unprecedented sensitivity. TGO began its science harvest in April 2018. A technique that has proved powerful for measuring the detailed composition of the Earth's atmosphere is solar occultation (e.g. ATMOS, ACE-FTS instruments). It was this mode of observation that primarily constrained the design of the mission and its atmospheric instruments, the Nadir, and Occultation for MArs Discovery NOMAD (NOMAD) and Atmospheric Chemistry Suite (ACS) instruments. Since then, tens of thousands of solar occultations have been executed continuously with four different channels: NOMAD-SO, and ACS-NIR/MIR/TIRVIM. The very high-sensitivity specification of these channels has greatly benefited the study of the vertical distribution of water vapor, enabling water to be identified to higher altitudes than with SPICAM, capturing water molecules up to 120 km in the most favorable cases (Belyaev et al. 2021). In addition, the space-time coverage of TGO solar occultations is a considerable improvement on MEx. With 24 occultation opportunities per day, and a pole-to-pole survey completed every Martian month (∼50 sols), TGO coverage outmatches the uneven MEx coverage, which is accomplished over restricted intervals of L_s ∼70° occurring twice a Martian year.

2.5 The Mars Express' Water Vapor Ambiguity: Reconciling Datasets

With the arrival of MEx and its simultaneous measurements of atmospheric water in several IR bands (near- and thermal-IR), some inconsistencies were identified. At the first MEx science conference in 2005, Vittorio Formisano, then PI of PFS, noted that the water vapor column abundance retrieved from PFS/SW at 2.56-μm was persistently larger than that retrieved at 30-μm with PFS/LW. He attributed this difference to the distinct vertical sensitivity of measurements between the two bands. SPICAM (1.38-μm) was lower than PFS/LW, and OMEGA (2.56-μm) was closer to PFS/SW. Opposite biases, unexplainable by aerosol impact, suggested there should be other reasons for the discrepancies. A dedicated ISSI (International Space Science Institute, Bern, Switzerland) team meeting gathered MEx water vapor experts in 2005 and 2006 (Korablev et al. 2006b) to verify retrieval techniques and assumptions used by different groups (Encrenaz et al. 2005; Fedorova et al. 2006) and compare the MEx retrievals to TES/MGS (Smith 2002, 2004), the reference dataset at that time. The team addressed spectroscopic parameters, *a priori* Mars atmospheric models, as well as solar lines. Homogenized procedures were then applied to selected MEx orbits where all the three instruments had operated simultaneously. Generally, a good agreement between datasets was found for the water northern peak (∼60 pr-μm) with the exception of SPICAM whose values were found slightly below PFS/LW (Fouchet et al. 2007). OMEGA and PFS/SW values were the largest (Maltagliati et al. 2008; Tschimmel et al. 2008). A reasonable agreement between PFS/SW and LW datasets was only found when the retrieval assumed that H_2O was confined near the surface (Tschimmel et al. 2008). One more output of the ISSI Team was a caveat found in the TES data pipeline that is detailed in Sect. 5.

Recently, Pankine (2022) compared PFS/LW with SPICAM IR (Trokhimovskiy et al. 2015), the two main MEx datasets available. Outside Global Dust Storm (GDS) periods, water vapor abundances retrieved in MY 27 and MY29 were found similar on average, except in the polar regions during summer and in the northern tropics during $L_s = 175$-210°. At these times and locations, SPICAM IR abundances were higher by 2-10 pr-μm. Pankine (2022) also shows that PFS/LW and SPICAM observations collected during MY27-29 remain systematically lower compared to TES observations made in MY25 and 26, with TES

abundances higher by a factor of almost two. Even though the MEx and TES datasets pertain to different epochs, the observed difference could not be attributed to interannual variability. Similarly, Mars Reconnaissance Orbiter (MRO)/Compact Reconnaissance Imaging Spectrometer (CRISM) water vapor abundances in MY29 (Smith et al. 2018) were found to be systematically higher by 50-100%. This disagreement is likely caused by differences in the water vapor absorption models and environmental parameters used in the retrievals (Pankine 2022).

3 Observing H & D Atoms in the Upper Atmosphere

3.1 SPICAM UV: Deriving H Abundance from Lym Lyman-α Observations

The ultimate source of atomic hydrogen in the Martian upper atmosphere (the Martian hydrogen corona) is the dissociation of the lower atmosphere water vapor, itself sourced from the polar ices (Maltagliati et al. 2013). Due to its low mass, atomic hydrogen can escape the gravity of Mars and escape into space, making it a proxy for estimating water escape from Mars. Water escape is a key process to understand Mars' climate evolution over ages. Unfortunately, H escape rate cannot be measured directly and can only be derived indirectly from atomic hydrogen observations. On Mars, the first estimate of H escape rate was made during the Mariner 6 and 7, and 9 missions using limb profiles of the Lyman-α optically thick emission of H (Anderson and Hord 1971; Anderson 1974). This Lyman-α emission is produced mainly by resonant scattering of solar Lyman-α photons by the hydrogen corona that surrounds Mars at distances of several Martian radii. SPICAM UV was able to observe this corona more than 30 years after the Mariner 6, 7 and 9 missions (Bertaux et al. 2005). Numerous limb observations were performed with SPICAM-UV (see Fig. 4). The first limb observations were limited to altitudes between 100 and 400 km to study the major dayglow emissions (Leblanc et al. 2006). The Lyman-α emission was detected throughout these observations, presenting a rather flat vertical profile at solar zenith angles (SZA) $< 83°$. Later, more extended observations reaching several thousands of km were dedicated to the study of the Lyman-α emission. These observations showed a decrease in the brightness above $\sim$500 – 1000 km, depending on the SZA (Chaufray et al. 2008).

These Lyman-α observations contain not only the Martian emission but also the emission due to the interplanetary hydrogen atoms that fill the interplanetary medium (*e.g.* Quémerais et al. 2013). This interplanetary emission is not uniform in the sky (Bertaux et al. 1995). It varies between $\sim$400 R to 800 R, which can represent a substantial fraction (from a few % to a few 10 s of %, depending on the SZA and altitude of the LOS) of the observed emission. This interplanetary emission needs to be subtracted from the limb observations to isolate the Martian emission. The MEx orbit was not elongated enough to directly sense this interplanetary emission. Thus, a model of the interplanetary emission, validated with the Lyman-α observations of the Solar Wind Anisotropies (SWAN) instrument onboard the Solar and Heliospheric Observatory (SOHO) mission, was used to estimate it (Quémerais et al. 2013).

Because the emission is optically thick in the altitude range of observations of SPICAM, the conversion of the Lyman-α brightness into hydrogen abundance is not straightforward. The analysis method is based on that presented by Thomas (1963) to study the Earth's hydrogen corona. It requires a simple parametrized model of the hydrogen density, and the use of a radiative transfer model able to consider the multiple scattering inside the hydrogen

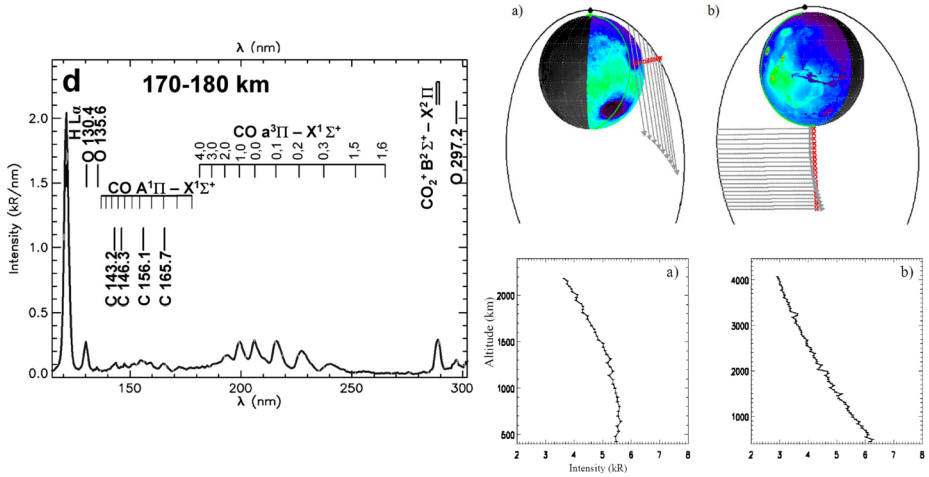

Fig. 4 From Leblanc et al. (2006) and Chaufray et al. (2008). (Left): example of spectrum observed by SPICAM in the dayside upper atmosphere of Mars at SZA between 14-37° and altitudes between 170 – 180 km. At these altitudes, the Lyman-α hydrogen emission line (121.6 nm) becomes dominant compared to the other dayglow emissions. Right top: Example of two geometries of observations of the Martian hydrogen corona observed at high altitudes at SZA = 30° (center) and SZA = 90° above the South Pole (right). Right bottom: Associated vertical profile of the H Lyman-α intensity for the two observations. Reproduced with permission; copyright by (top) Elsevier, (middle) AGU, (bottom) ESO

corona. This model then simulates brightness for different viewing configurations and states of the Martian exosphere.

The study of the first 7 vertical profiles measured near Ls = 180° at SZA ∼30° and ∼90° used a two parameter 1D model of the hydrogen density from 80 km to 50,000 km (Chaufray et al. 2008). This first study derived an average hydrogen density at the exobase of $\sim 1.8 \times 10^5$ cm^{-3} and a temperature of 230 K. But it also showed that given their limited altitude range, the observations could be reproduced by various solutions in the parameter space, leading to relatively large uncertainties in these derived parameters. In addition, the systematic uncertainty due to instrument calibration, and the choice for the solar flux at 121.6 nm was found to be a major source of degeneracy in the derived exospheric temperature. In particular, this degeneracy comprises the possibility to have two populations of atoms to explain observations (Chaufray et al. 2008). A larger set of 21 observations during the second half of 2007 (Martian year 28) was studied later by Chaffin et al. (2014) using a similar approach to derive the hydrogen abundance. Their results, which show an unexpected seasonal variation of the hydrogen abundance and escape rate, are discussed in more depth in Sect. 8 along with the perspectives they have opened for water escape on Mars. Another set of ∼100 SPICAM observations during the Martian years 28 and 29 was used and compared to some simulated brightness with a 3D model to study these seasonal variations (Chaufray et al. 2021a).

3.2 The Imaging Ultraviolet Spectrograph (IUVS): Deriving D Abundance from Lyman-α Observations

The study of water escape from Mars has been supplemented with D Lyman-α observations using the Hubble Space Telescope and IUVS on the Mars Atmosphere and Volatile Evolution (MAVEN) missions (Jakosky et al. 2015). The Hubble Space Telescope (HST) and

MAVEN each have an echelle high-resolution observing mode that can spectrally resolve the D and H Lyman-α emissions at 1215.35 Å and 1215.67 Å, respectively (McClintock et al. 2015). The abundance of D at Mars is much smaller than H, making the resulting D Lyman-α brightness much fainter than that of H Lyman-α (Krasnopolsky et al. 1998). Dedicated observations of D made throughout the MAVEN mission timeline measured D atoms up to ~300 km above the surface, compared with H atoms that could be measured to several Mars radii (Mayyasi et al. 2019; Bhattacharyya et al. 2015). The D emission can be converted to estimated abundances (densities) using a radiative transfer model with a parametrized vertical profile as for H. Because the emission is optically much thinner than H, the derived D abundance is linearly dependent on the absolute calibration and its uncertainty is easier to evaluate. The D Lyman-α measured by MAVEN between Ls = 220° and Ls = 340°, at limb near ~200 km is of a few 100 s Rayleigh (Mayyasi et al. 2018; Bhattacharyya et al. 2020) and then should contribute up to ~10% to the Lyman-α emission observed by SPICAM at this season near this altitude, but should be negligible above 400 km (Chaufray et al. 2021b). At other seasons, for example near aphelion, HST measured only a much weaker emission of ~20-50 R (Krasnopolsky et al. 1998) which represents less than 1% of the H emission.

Both D and H emissions showed seasonal variability where solar insolation and regional dust storms, occurring around the Southern Summer season, lead to large-scale convection that inflates the atmosphere and causes more D and H atoms to reach higher altitudes (Mayyasi et al. 2017, 2023). The subsequent density retrievals can be used to estimate the D/H ratio in the upper atmosphere of Mars (Clarke et al. 2024). The D/H ratio is used as a metric to compare with the HDO/H_2O ratio in the lower atmosphere, as well as with other planets and solar system bodies to evaluate the primordial water content at Mars and throughout the Solar System (Jakosky 2021).

4 The Source(s) of Water

4.1 The NPC: A Massive Reservoir for H_2O

The North polar region of Mars has long been known to host a massive reservoir of water ice whose surface can exchange directly with the atmosphere (Fig. 5-left). It is understood now that this reservoir, the North polar cap (NPC) is the main, if not the only, supplier of atmospheric water on a seasonal basis (Montmessin et al. 2017a). The NPC produces a factor of two increase in global abundance when exposed to the Sun in spring and summer (Smith 2002).

The Mars Advanced Radar for Subsurface and Ionospheric Sounding (MARSIS) radar observed ice-rich deposits in the northern polar region, including the NPC and the north polar layered deposits (NPLD) (Picardi et al. 2005; Fig. 5-right). Observations revealed the NPC to be the upper part of the extensive ~2-km-thick NPLD, overlaying a much dustier and older (billion years old) Basal Unit (BU). The combined volume of water ice in these deposits was estimated to be $\sim 1.3 \times 10^6$ km^3 (Selvans et al. 2010).

4.2 Seasonal Frost Cycle

The seasonal CO_2 north polar cap reaches its maximum areal extent around the start of northern winter at $L_s = 270°$ (Piqueux et al. 2015). The seasonal cap gradually decreases in extent through winter and spring, and completely disappears by $L_s \sim 80°$. OMEGA observed the

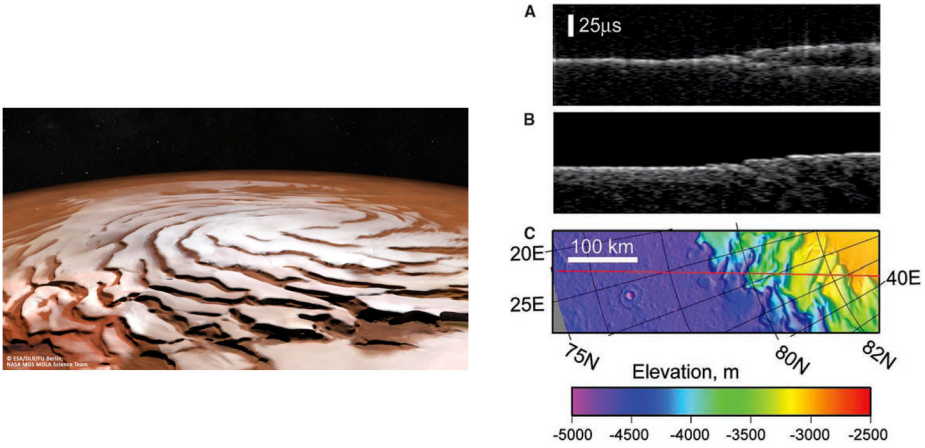

Fig. 5 (Left) High Resolution Stereo Camera (HRSC) color image mosaic, created out of 32 orbit stripes, yielding a perspective of the northern ice cap. Mosaic created by the Planetary Sciences and Remote Sensing group at Freie Universität Berlin. (Right) (A) MARSIS data as it crossed the margin of the NPLD. (B) Simulated MARSIS data if echoes are only from the surface (nadir and off-nadir clutter). (C) MOLA topography along the ground track (red line). Reproduced with permission from Picardi et al. (2005), copyright by AAAS

retreat of the north seasonal cap during MY27-28 and uncovered a complex picture of the evolution of the seasonal water ice and the CO_2 deposits (Langevin et al. 2005; Appéré et al. 2011). A water ice annulus several degrees of latitude wide forms near the edge of the CO_2 seasonal cap during winter. This deposit first consists of thin frost and then is overlaid with water ice grains released from the sublimating CO_2 ice layer. By L_s ~50°, the spectral signature of the water ice dominates the seasonal cap. Appéré et al. (2011) interpreted this observation by the OMEGA instrument as the evidence of an optically thick layer of H_2O ice forming on top of the remaining seasonal CO_2 deposit by the release of water ice grains from the CO_2 ice and by the cold trapping of the water vapor sublimated from the water ice annulus. At some locations where CO_2 signature previously decreased, it increased again between $L_s = 40\text{-}70°$, suggesting local removal of the water ice layer. The emerging picture is that of a very dynamic exchange between the surface frost and the atmosphere vapor at the north polar region during spring.

4.3 The North Polar Cap Sublimation Season

The OMEGA, PFS and SPICAM instruments on MEx presented a consistent picture of atmospheric water vapor gradually increasing through northern spring at latitudes south of the edge of the seasonal cap (Encrenaz et al. 2005; Fouchet et al. 2007; Melchiorri et al. 2007; Tschimmel et al. 2008; Trokhimovskiy et al. 2015; Pankine 2022). A region of relatively high vapor abundances forms in the atmosphere just south of the edge of the retreating seasonal cap, starting at L_s ~30-45° (Pankine et al. 2010). PFS/LW confirmed that this circumpolar ring of vapor also formed during the MEx mission (Pankine 2022).

After L_s ~80°, the north polar cap is clear of seasonal frost and water ice in the cap can sublimate, releasing vapor into the atmosphere. This leads to a dramatic increase in vapor abundances in the polar atmosphere in early summer. Various MEx instruments observed the highest vapor abundances of ~40-70 pr-µm in the northern polar region at L_s ~100-110°, qualitatively consistent, but systematically lower than previous observations by the MGS

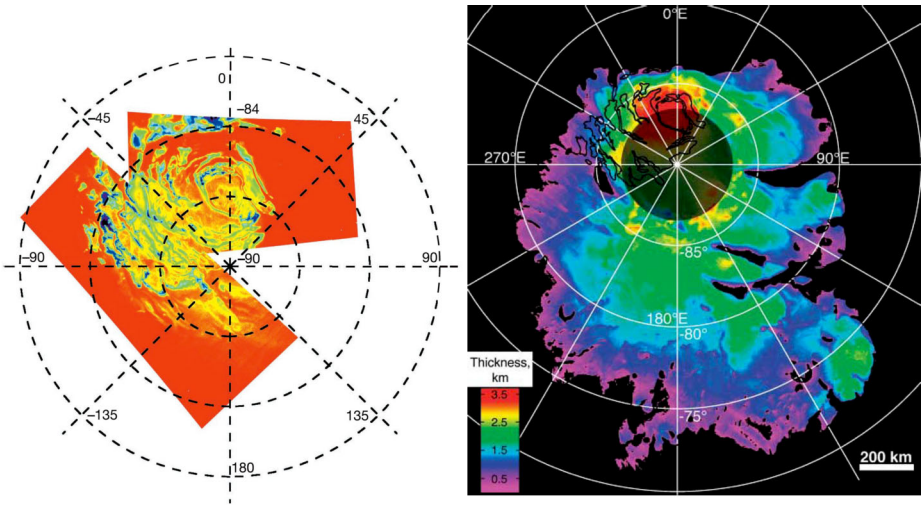

Fig. 6 (Left) Polar map of H2O ice at the South Pole of Mars. H2O absorption feature observed by OMEGA, from blue (deep absorption) to red (ice-free). From Bibring et al and reprinted with permission from Springer Nature. (2004). (Right) MARSIS data and MOLA topography showing thickness of the SPLD. Red-color areas near the South Pole correspond to the thickest part of the SPLD and occur beneath the highest elevations. MARSIS also revealed SPLD as a vast deposit of dusty water ice extending ∼300 km from the pole and reaching thicknesses ∼3.7 km. The SPLD are currently buried under a layer of sand and appear to be isolated from the current water cycle. Reproduced with permission from Plaut et al. (2007), copyright by AAAS

TES (Smith 2004; Tschimmel et al. 2008; Pankine et al. 2010). Models (Houben et al. 1997; Richardson and Wilson 2002a; Montmessin et al. 2004, 2017a) show that some of that water condenses on the ground as seasonal frost at mid-to-high latitudes during late summer and fall, while some is transported to the tropics. The frost sublimates during winter and spring, is transported poleward and is re-deposited on the cap in late spring, recycling water back to the pole.

Thanks to its imaging capability, OMEGA has been able to map the sublimation of water vapor above the polar caps at summer solstice (Melchiorri et al. 2007, 2009). A map of the column abundance above the North Pole Region for $L_s = 106 – 110°$, at the time of its maximum sublimation, could be derived, showing a local maximum at latitudes 75 – 80°N and longitudes 210-240°E, not far from the region where OMEGA identified calcium-rich sulfates (likely gypsum).

4.4 The South Pole of Mars: Another Reservoir of Water?

In 2004, the OMEGA instrument on MEx discovered water-ice patches exposed at the South Pole of Mars after the complete sublimation of the seasonal water ice frost (Bibring et al. 2004; Fig. 6), complementing the finding of TES (Titus et al. 2003). These patches could be spotted in the surroundings of the residual CO_2 ice cap, as well as within the cap itself. The residual south polar CO_2 cap may be acting as a permanent sink of atmospheric water vapor; Langevin et al. (2007) reported water ice being deposited on the cap during summer. Climate model simulations were then used to tentatively explain this residual water ice; proposing that recent climate changes ($<$ 100 kyr) may have been conducive for thick water ice deposition beneath the CO_2 ice cap (Montmessin et al. 2007).

4.5 The Role of the Regolith

Water ice in the shallow subsurface and water adsorbed in the regolith may potentially represent a meaningful reservoir of water on Mars (Zent et al. 1993; Böttger et al. 2005). There is compelling evidence that subsurface ice is present at shallow depth (0.5-1 m) in Martian mid- and high latitudes (Mitrofanov et al. 2004; Maurice et al. 2011). This water ice can diffuse through overlaying regolith and contribute to atmospheric water on diurnal or seasonal scales (Zent et al. 1993; Böttger et al. 2005).

The OMEGA instrument mapped H_2O- and OH-bearing phases in the surface regolith and rocks using a 3-μm absorption band in NIR reflectance spectra (Milliken et al. 2007). OMEGA observations were consistent with surface water content of 4 ± 1 wt% at the equator and mid-latitudes, and 6-10 wt% at the poles (Audouard et al. 2014). However, the lack of temporal variability in the retrieved surface hydration and the lack of correlation with atmospheric relative humidity suggested that this water is not easily exchangeable with the atmosphere. The surface water is likely to be strongly bound to minerals and amorphous components in the Martian regolith, or it could be that the low present-day temperatures make dehydration and rehydration a very slow process (Audouard et al. 2014).

At the same time, OMEGA observations of atmospheric vapor abundances at the South Pole Region during Ls = 250-270°, outside the CO_2 polar cap, detected an increase of a few precipitable microns during the day (Melchiorri et al. 2009). Fouchet et al. (2007) also showed that PFS/LW retrievals could not be explained by a well-mixed water vapor abundance. The best law describing the PFS/LW water column density as a function of pressure, H_2O (pr-μm) = a + b × Psurf (Pa), needed to include a pressure-independent "background" water column of typically 3–4 pr-μm, suggesting surface-atmosphere exchange. A possible scenario includes exchanges of vapor with the regolith that could gather water from the atmosphere, adsorbing the water into the surface during the nighttime and desorbing it as soon as the Sun reaches sufficient height to heat the ground. This hypothesis is even more plausible considering the presence of observed local enhancements in the morning sections associated with the illumination of the Sun and the total absence in the data for water ice (Melchiorri et al. 2009). It should be noted that numerical simulations of the Martian water cycle can reproduce observed seasonal variability of atmospheric water vapor without the need for an exchangeable surface reservoir of water outside the polar regions (Montmessin et al. 2004). Despite numerous attempts to explore its effect locally (Zent et al. 2010; Savijärvi et al. 2016; Steele et al. 2017; Fischer et al. 2019; Tamppari and Lemmon 2020; Savijärvi and Harri 2021; Polkko et al. 2023; Leung et al. 2024), the global role of the regolith has not been elucidated and remains a highly elusive component of the water cycle.

5 The Seasonal Evolution of Water Column Abundance

5.1 The Mars Express Climatology Legacy

All the MEx instruments that have monitored the seasonal and latitudinal variations of water vapor column abundance (Fedorova et al. 2006; Fouchet et al. 2007; Trokhimovskiy et al. 2015; Montmessin et al. 2017b; Pankine 2022) have mostly confirmed previous surveys reported from TES and MAWD data. In summary, the annual cycle of water vapor has an evolution marked by the northern spring/summer release of water vapor from the north polar cap, a stark reduction of water at mid-to-high latitudes during fall and winter, and a moderate pulse of water from the south polar region in summer (Smith 2002). Disparities in column

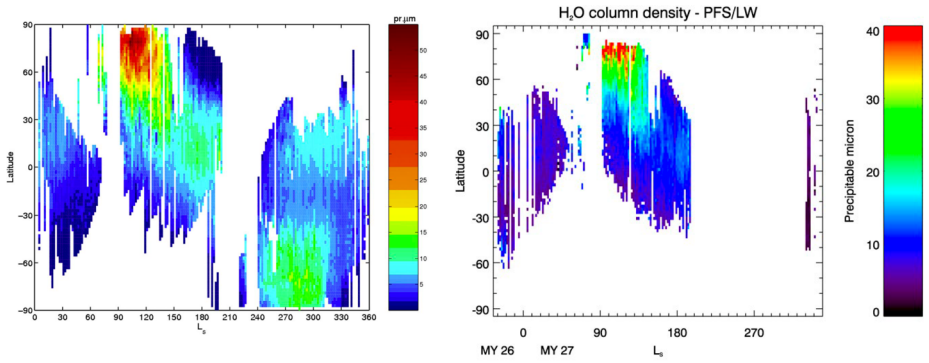

Fig. 7 The seasonal evolution of water column abundance as seen by SPICAM (left, from Fedorova et al. 2006 and reprinted with permission from Wiley), and PFS (right, from Fouchet et al. 2007 and reprinted with permission from Elsevier) from the end of MY26 to the end of MY27

values (see Sect. 2) between instruments have not been fully explained to date, but are likely caused by the different ways the atmosphere is probed between the TIR and the NIR spectral domains.

5.2 Revising Previous Climatologies

Fedorova et al. (2006) published the first MEx annual survey (end of MY26 + MY27, Fig. 7-left), based on the "MAWD-like" method, using the 1.38 µm feature of water sensed by SPICAM. Using PFS, Fouchet et al. (2007) delivered soon after a similar climatology (Fig. 7-right), this time in a "TES-like" configuration (using thermal IR bands). Fedorova et al. (2006) revealed a drier cycle compared to TES and MAWD, with differences as high as a factor of two. However, the original MAWD retrievals relied on outdated spectroscopy that contained half as many water lines in the 1.37 µm region compared to the SPICAM retrieval. This led to a subsequent revision of MAWD data by Fedorova et al. (2010) that brought the MAWD and SPICAM datasets in much better agreement.

As alluded to earlier, Fouchet et al. (2007) also found a systematic disagreement (a factor of ∼1.5) between PFS and TES that both sensed water vapor the same way, that is from the thermal emission of the atmosphere and the surface in the 20-35 µm range. Fouchet et al. (2007) discussed private communications with M.D. Smith, responsible for TES retrievals, that revealed a disagreement between measurements made by TES with two spectral resolution modes; the coarser one yielding systematically higher values and inconsistent retrievals between the various water lines. Therefore, a plausible explanation was found that helped reconcile the MEx era with the pre- MEx era measurements, implying that Mars' water cycle had remained stable for decades.

Tschimmel et al. (2008) used the short-wavelength (SW) channel of PFS that captures water vapor absorption at 2.56 µm and presented a comparison with other instruments that revealed a systematic underestimation by SPICAM relative to the others, while also showing that the PFS TIR channel produced higher values compared to its SW counterpart. A strong discrepancy between the two channels was found during the northern summer northward of 50°N that the authors tentatively attributed to near-surface confinement of water vapor.

Meanwhile, OMEGA also used the 2.6-µm band of H_2O (Maltagliati et al. 2011). The seasonal behavior appears in good agreement with past and simultaneous retrievals both qualitatively and quantitatively, within the uncertainties. The average water vapor abundance

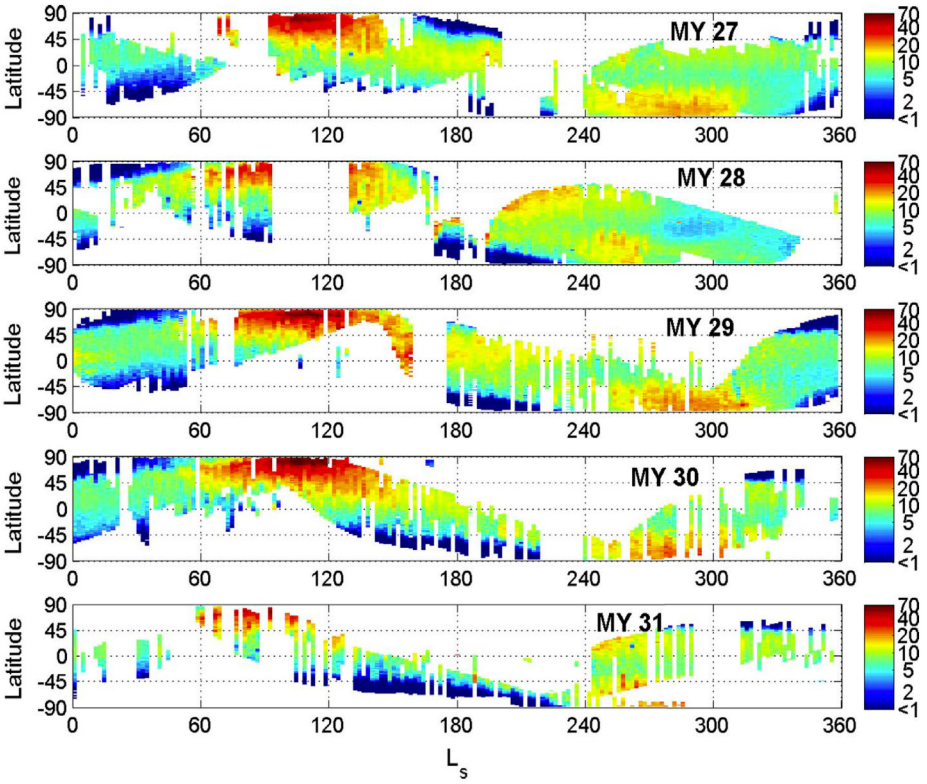

Fig. 8 SPICAM multiannual survey of water vapor column abundance spanning the MY27 to 31 period. Reproduced with permission from Trokhimovskiy et al. (2015), copyright by Elsevier

during the year was found to be pr-μm, with an imbalance between northern and Southern Hemisphere, in favor of the first. The maximum of activity, up to 60 pr-μm, occurs at high northern latitudes during local summer and shows the dominance of the northern polar cap within the driving processes of the water cycle. A corresponding maximum at southern polar latitudes during the local summer is present, but less structured and intense, with a maximum value of 25 pr-μm.

Together with CRISM (Smith et al. 2018); one of the longest MEx climatologies for water vapor can be found in Trokhimovskiy et al. (2015, Fig. 8). Compared to Fedorova et al. (2006), Trokhimovskiy et al. (2015) implemented several improvements; in particular the scattering by dust and clouds based on the opacity data of Mars Odyssey/THEMIS (Smith et al. 2009). They found that multiple scattering by aerosols can increase the retrieved water vapor amount by up to 10% at the summer poles, and up to 60-70% for large solar zenital angles. The impact of surface albedo, solar spectrum, and water vapor vertical distribution was also addressed in this work. No significant interannual variation was found, in agreement with TES (Smith 2004), except for a decrease concomitant with the MY28 global dust storm that could not be explained by increased dust opacity and subsequent column masking.

OMEGA was also used to study the seasonal behavior of water vapor above the Hellas basin, where measurements are made easier by the higher surface pressure (Encrenaz et al.

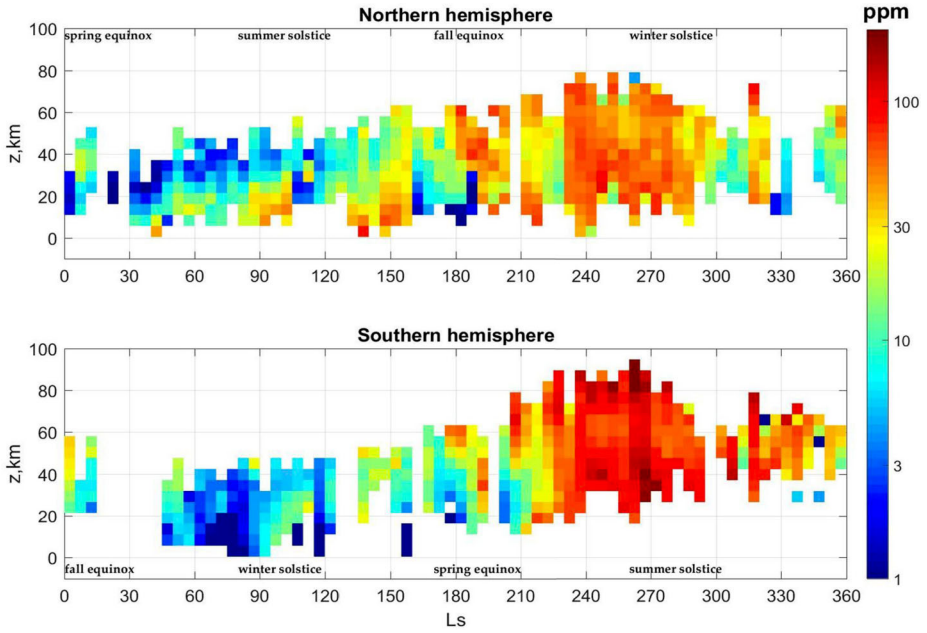

Fig. 9 The multiannual (GDS years excluded) mean of H_2O mixing ratio (in ppmv) vs. altitude and L_S in both hemispheres. The L_S scales are shifted to align summer and winter in both hemispheres. Altitudes and L_S are arranged into 5 km × 5° bins. Reproduced with permission from Fedorova et al. (2021), copyright by AGU

2005). The H_2O column density is found to range from very low values (between southern fall and winter) up to more than 15 pr-μm during southern spring and summer.

6 Analyzing the Vertical Distribution of Water: A New Paradigm

6.1 The Changing Behavior of Water Vapor Altitude Distribution

SPICAM IR was the first spectrometer to provide long-term monitoring of the water vapor vertical distribution across more than 8 Martian years. Two occultation campaigns of MY29 were studied in Maltagliati et al. (2011, 2013), resulting in two discoveries: supersaturation of water in the aphelion season (2011) and high-altitude water during perihelion (2013). SPICAM IR was also the first spectrometer to observe the water vertical distribution during the Global Dust Storm of MY28 and found water at very high altitude, up to 100 ppmv at 80 km in these dust events (Fedorova et al. 2018).

Figure 9 shows the seasonal behavior of water vapor mixing ratio observed by SPICAM from MY28 to MY34 (Fedorova et al. 2021). During aphelion, water is confined below 40-60 km for all Martian years observed. The highest altitude where water vapor can be spotted is between 70 and 90 km during perihelion season, nearly accessing the upper atmosphere. In this season, years without GDS show a significant moistening of the upper atmosphere (∼100 ppmv) in the Southern Hemisphere, with likely seasonal impact on hydrogen escape. SPICAM observation allowed for the comparison of the water distributions during two observed GDS, in MY28 and MY34, that showed a substantial disparity in water

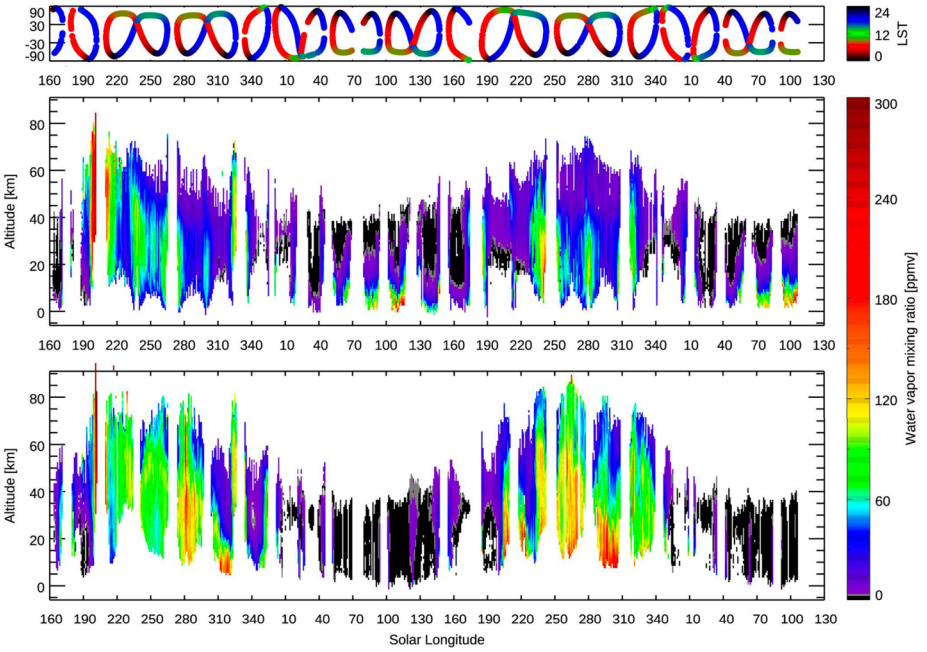

Fig. 10 Seasonal variation of the water vapor vertical profiles from Ls = 160° in MY 34 to Ls = 330° in MY36 obtained from the TGO/NOMAD solar occultation measurements taken in the Northern Hemisphere (the middle panel) and the Southern Hemisphere (the bottom panel). Data are binned into intervals of 1° of L_S. The top panel shows the latitudes and local solar time of the measurements. Reproduced with permission from Aoki et al. (2022), copyright by the authors

vapor response. The storm in MY28 began at Ls = 270, which coincides with the southern summer solstice, creating the largest excess of water in both hemispheres at >80 km.

Since 2018, a daily monitoring of H_2O vertical distribution has been performed by NOMAD and ACS solar occultation measurements. Thanks to high spectral resolving power and sensitivity, the instruments enabled an in-depth study of water vapor vertical distribution from the surface up to 120 km thanks to the use of different spectral bands (Aoki et al. 2019, 2022; Belyaev et al. 2021; Fedorova et al. 2020, 2023; Villanueva et al. 2021, 2022; Brines et al. 2023). Figure 10 shows the seasonal variation of water vapor vertical profiles obtained from two Martian years' operation of the NOMAD solar occultation measurements (see Aoki et al. 2019, 2022; Brines et al. 2023; Vandaele et al. 2019; Villanueva et al. 2021, 2022 for details). Such a wide vertical coverage is achieved by combining strong and weak water bands at 2.56 and 3.3 μm that have different sensitivities in altitude. Figure 10 shows that NOMAD agrees well with SPICAM, especially for the strong contrast between aphelion and perihelion water behavior. This panel reveals that water vapor is confined to low altitude (below 10-20 km) around aphelion while it accesses and populates the mid-to-high atmosphere (>40 km) during perihelion. Based on observations of MY34 and 35, 10-50 ppmv can be found up to 120 km during GDSs and perihelion (Belyaev et al. 2021). High altitude water up to 100 km was also observed by SPICAM, ACS and NOMAD (Fig. 1 and 2) during the regional C storm that occurs every Martian year around Ls = 330°. This dust event likely plays a role in water escape, as it produces a surge of escaping hydrogen atoms in the exosphere (see Sect. 8). The contribution of the MY34 GDS was found to be equivalent to

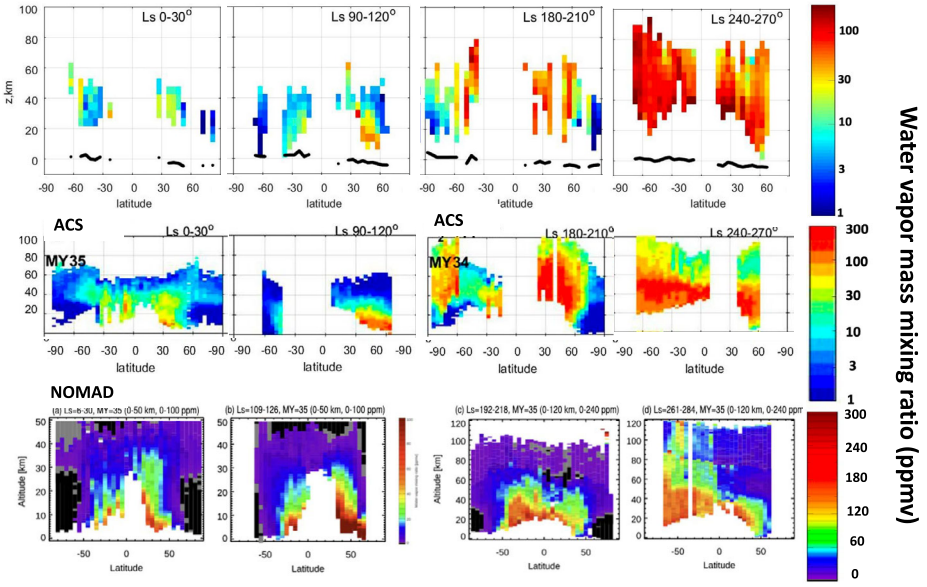

Fig. 11 Latitudinal variation of the water vapor volume mixing ratio (in ppmv); vertical profiles are averaged over four periods of Ls, comprising equinoxes (0°, 180°) and solstices (90°, 270°). The three rows show from top to bottom: SPICAM, ACS, NOMAD results. Reproduced with permission from (top, middle) Fedorova et al. (2021, 2023), copyright by AGU; and (bottom) from Aoki et al. (2022), copyright by the authors

each of the perihelion periods of MY34 and 35 for the high altitude production of hydrogen (Belyaev et al. 2021; Montmessin et al. 2022).

Figure 11 shows the latitudinal distributions of water vapor for the four seasons, as observed by SPICAM, ACS, and NOMAD. Around equinoxes, water is confined to the low-to-mid latitudes, while polar regions remain dry. During northern summer, water vapor sublimates massively from the NPC and creeps towards the equator while being confined near the surface. This near-surface confinement is reminiscent of the boundary layer clouds observed by the Phoenix mission at the same period (Whiteway et al. 2009). In the mid-to-low latitudes, a vertically deep Hadley cell carries water from North to South, yet water remains confined low as it is capped by the aphelion cloud belt (Montmessin et al. 2004; Kahre et al. 2020). In stark contrast, water vapor sublimating from the south polar region during perihelion reaches very high altitudes. There, the atmosphere is warm enough to prevent cloud formation, which, combined with the intensified perihelion circulation, enables rapid propagation at high altitude.

6.2 The Saturation State of Water

Condensation is a major process constraining the vertical distribution of water on Mars. However, condensation can only proceed after ice nucleates onto dust particles, which thus requires considering the water vapor saturation state. When dust nuclei are too scarce or when growth is hampered by low pressure and temperature; condensation can become ineffective at keeping water vapor at saturation, and large supersaturation can potentially build up.

Maltagliati et al. (2011) reported the first evidence of supersaturation on Mars based on SPICAM data collected during aphelion at low-to-mid latitudes of both hemispheres. There,

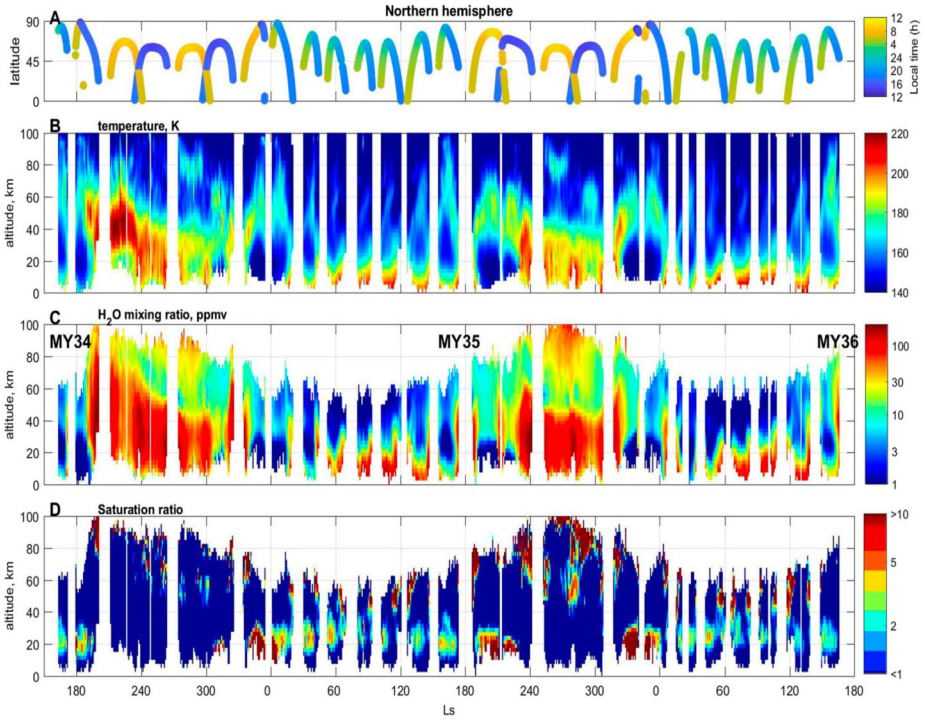

Fig. 12 Seasonal variation of temperature (B), water vapor (C) and saturation ratio (D) profiles from Ls = 163° of MY34 to Ls = 170° of MY36 retrieved from the ACS NIR data in the Northern Hemisphere. The retrieval was binned into intervals of 1° of L_S and 2 km of altitude. The top panel shows the latitudes and local time of the measurements. Reproduced with permission from Fedorova et al. (2023), copyright by AGU

the saturation ratio was observed to reach 2 to 10 at an altitude of 30–40 km. To evaluate saturation, both water vapor concentration and temperature must be known, the latter not being measured by SPICAM. The saturation state could, however, be derived thanks to collocated Mars Climate Sounder (MCS) temperatures corrected for local time (Kleinböhl et al. 2009).

Supersaturation has been explained by a lack of dust nuclei due to dust being scavenged by forming and subsequently sedimenting ice particles. Fedorova et al. (2014), analyzing the same set of observations as Maltagliati et al. (2011), have shown that aerosols were actually present but mostly in the form of sub-micron particles of ($r_{eff} < 0.1$ μm). The saturation ratio necessary to trigger nucleation for such small particles can vary from 2 to 4 in the colder middle atmosphere, consistent with the supersaturation levels observed by SPICAM.

With TGO solar occultations, both temperature and water vapor concentration can be simultaneously retrieved (Fig. 12). ACS and NOMAD have been able to construct independently the seasonal variations of the saturation of water vapor from 0 to 100 km (Fedorova et al. 2023; Brines et al. 2023). It was found that water is often supersaturated above the dust layer, reinforcing the idea that dust serves as cloud nuclei. At aphelion in low-to-mid latitudes, water above 40 km is supersaturated. Furthermore, supersaturation was found in both polar regions below 20-30 km near equinoxes, where water vapor advected from low latitudes meets the cold polar vortex. Around perihelion, water is also supersaturated above 60 km in both hemispheres (Fedorova et al. 2020; Brines et al. 2023). This was supported by Mars Assimilated Remote Soundings (OpenMars) (Holmes et al. 2021, 2022) which show

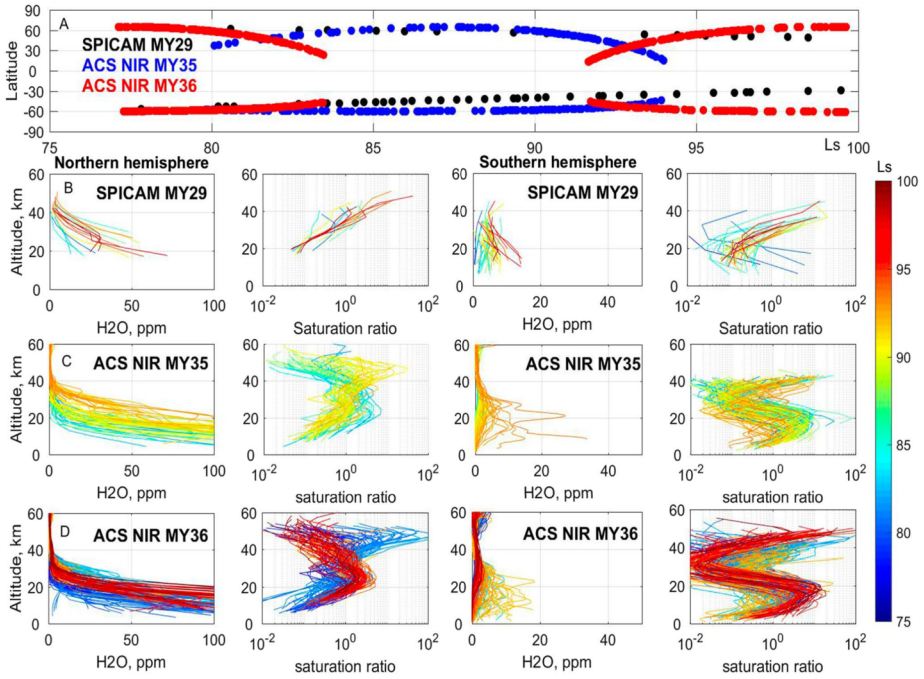

Fig. 13 Water vapor vertical profiles and saturation ratio obtained by SPICAM IR in MY29 (B) and ACS NIR in MY35 (C) and MY36 (D) at Ls = 75°-100° in northern and southern hemispheres. Panel A presents the latitudinal coverage of occultations. From Fedorova et al. (2023) and reprinted with permission from Wiley

discrete layers of supersaturation above 60 km at all latitudes during the MY34 dusty season.

The coverage of TGO solar occultations allowed comparing the water saturation obtained by SPICAM in MY29 at Ls = 50°-120° with that of ACS NIR in MY34 and MY35 (Fig. 13). The two experiments have shown good consistency despite the low sensitivity and vertical resolution of SPICAM, thereby demonstrating the repeatable nature of supersaturation.

6.3 Combining PFS and SPICAM to Study Water Confinement

The near-surface water vapor concentration has long eluded orbital investigations. It is generally not possible to probe near-surface water by solar occultation, as signal sensitivity decreases considerably below 10 km due to increasing aerosol line-of-sight opacity with decreasing altitude. Nadir observations, on the other hand, are limited by the available information content; with a degree of freedom (DOF) of the retrieval usually fluctuating around 1, only one parameter regarding the column of water can be retrieved, normally the column-integrated abundance (see Fig. 3 in Knutsen et al. 2022). This limitation can be overcome by using co-located measurements of H_2O performed at separate wavelength intervals (such as with SPICAM and PFS) as long as the sensitivity to various regions of the column differs between the two intervals (Fig. 14a and 14b). This technique was tested and validated in Montmessin and Ferron (2019), and applied to the entire available MEx set of co-located measurements from SPICAM and PFS in Knutsen et al. (2022).

Water vapor inversion carried out in a single operation, after combining the two intervals into a single "synergistic" spectrum, results in a vertical profile such as that shown

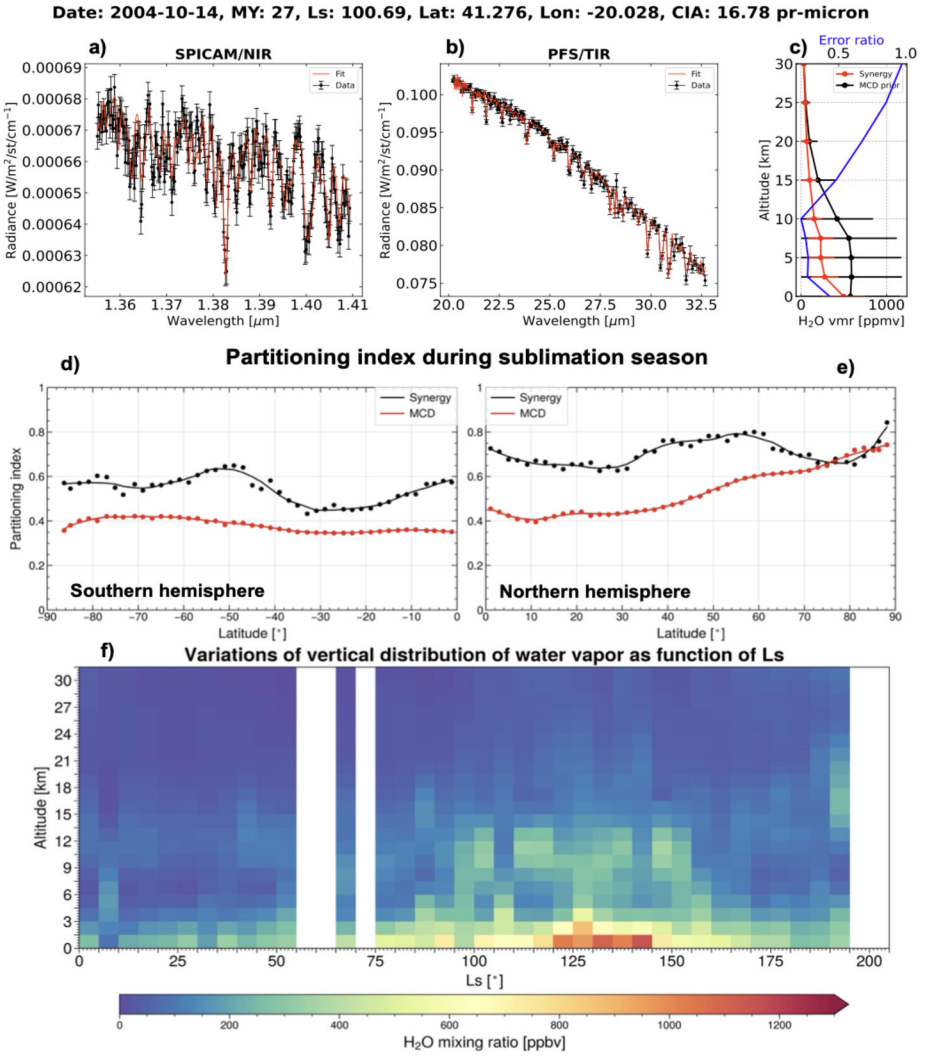

Fig. 14 A summary of the synergy inputs and outputs: a)-b) Average of 15/9 consecutive SPICAM/PFS spectra (black) with best fit (red), c) example of retrieved vertical profile (red), MCD a priori profile (black) and retrieved-prior error ratio, d)-e) the average Partitioning Index (see text for its definition) for both synergy (black) and MCD (red) covering the sublimation season for each hemisphere (Ls = 255°–315° for the SH and Ls = 75°–135° for the Northern Hemisphere), f) temporal cross-section showing average vertical distribution of H_2O from latitudes 30-45°N. Reproduced with permission from Knutsen et al. (2022), copyright by the authors

in Fig. 14c. For a significant portion of the MEx dataset, the DOF is more than doubled, allowing information about the vertical distribution to be extracted, whereas the separate retrievals from the two wavelength intervals could only be interpreted in terms of mutual (in)consistency (like when the MEx cross-comparison exercise was conducted at ISSI).

The retrieval itself consists in adjusting evenly spaced water concentration parameters bound by a high correlation length (∼a scale height) along the vertical, using an optimal estimation method. The prior estimators of water parameters are extracted from the Mars Climate Database (MCD) v5.3 (Millour et al. 2017), while their prior uncertainty is set to a fixed value. An idea of whether and how much information is injected by the synergistic spectrum into the retrieval can be assessed by considering the ratio between the posterior (retrieved) and the prior errors. A ratio less than one indicates that the synergistic measurement supplies new information, the depth of which being gauged by how much smaller the ratio is compared to one. Compared with single-interval retrievals, synergy demonstrates enhanced sensitivity to the lowest part of the atmosphere (Knutsen et al. 2022).

Synergy also provides more accurate column abundances while being overall in agreement with single-instrument observations and the MCD (Fig. 7 of Knutsen et al. 2022). What makes synergy unique is the retrieved information on near-surface water vapor. The Partitioning Index (PI) parameter provides a measure of the vertical confinement; namely, the fraction of water lying below 5 km compared to the full column (Fig. 14d-14e). While synergy and MCD agree on column-integrated abundances (yet with a lower polar sublimation peak in the Northern Hemisphere), their PI differs significantly (Fig. 14d and 14e). In addition to an overall stronger confinement near the surface compared to the MCD, the synergy also suggests an unpredicted detached vapor layer at 12 km altitude (Fig. 14f) in Northern summer. Finally, it should be stressed that MEx is the only platform orbiting Mars with a potential for water vapor synergy.

7 From Water to Escaping H

Perhaps one of the most disruptive findings regarding the fate of water on Mars was deduced from the MEx UV observations of the so-called hydrogen corona that is located in the upper thermosphere and up into the exosphere and that is populated by H atoms sourced by the photochemical decomposition of water vapor. H atoms are the sole escape carrier for water and are thus key to understanding water evolution on Mars.

7.1 Hydrogen Production: A Paradigm Shift

After the Mariner missions, a flawed understanding developed that H loss to space would not vary on shorter than decadal timescales. Before these missions, some speculated that seasonal variation in upper atmospheric hydrogen might be observable due to variations in the lower atmosphere water abundance (Barth et al. 1969; Hord et al. 1970). However, early analysis of the Mariner 6, 7, and 9 ultraviolet spectrometer data demonstrated a remarkable consistency in the upper atmosphere hydrogen brightness profiles, which was interpreted as a near-constant loss of H to space (Anderson and Hord 1971; Barth et al. 1972; Anderson 1974). Since theory predicted that photolysis in the lower atmosphere would result in non-condensable molecular hydrogen (McElroy and Donahue 1972; Parkinson and Hunten 1972), an orthodox view of H loss developed in which water was confined by condensation at relatively low altitudes all year long (Clancy et al. 1996). In this view, H_2 becomes the dominant H carrier above the condensation level and into the upper atmosphere. The long photochemical lifetime of H_2 ($>$30yr) provides a long-term buffer against seasonal, interannual, and solar cycle variations. This led to the assumption that H loss is diffusion limited at the bottom of the thermosphere (Hunten 1973), and remains constant over seasonal and decadal timescales (Zahnle et al. 2008).

Observations from both the Hubble Space Telescope (Clarke et al. 2014) and SPICAM (Chaffin et al. 2014) challenged this classical perspective. They demonstrated that large variations in the upper atmospheric hydrogen brightness implied escape rates too large and too variable to be supported by molecular hydrogen production alone. As the majority of hydrogen in the Mars atmosphere is present in water, these observations strongly suggested that water was at times able to bypass the cold trap and directly supply H to the upper atmosphere. This echoes the observations of large and occasionally supersaturated water abundance in the upper atmosphere by MEx/SPICAM Maltagliati et al. (2011, 2013). Later observations by HST confirmed that the variation was seasonal (Bhattacharyya et al. 2015), with loss rates peaking in southern summer. Photochemical modeling demonstrated that the water concentrations observed in the middle atmosphere could boost hydrogen loss on subseasonal timescales to rates consistent with those derived from upper atmospheric observations (Chaffin et al. 2017).

Subsequent observations (Bhattacharyya et al. 2015, 2017; Clarke et al. 2017; Halekas 2017; Rahmati et al. 2017; Heavens et al. 2018; Mayyasi et al. 2019; Stone et al. 2020; Chaffin et al. 2021; Qin 2021) and modeling (Krasnopolsky 2019; Shaposhnikov et al. 2019; Neary et al. 2020; Holmes et al. 2021; Chaufray et al. 2021a) cemented middle/upper atmospheric water as the source of seasonally enhanced H loss and began to investigate driving mechanisms. Work by Shaposhnikov et al. (2019) and Neary et al. (2020) using Mars general circulation models demonstrated that the seasonal Hadley circulation is capable of lifting water vapor to high altitudes as part of the interhemispheric transport. In southern summer, higher insolation and the hemispheric topographic asymmetry intensify upward mixing and transport rates, resulting in much more water in the middle atmosphere near southern summer solstice; H loss rates to space peak close to solstice and well after perihelion (Bhattacharyya et al. 2015; Halekas 2017). According to Richardson and Wilson (2002b), the topographic asymmetry is more important than the timing of perihelion in producing the climatic asymmetry between Northern and Southern summer observed at present.

7.2 Hydrogen Escape: What's Left to Understand

Despite these advances, knowledge of the processes that drive H loss to space today and throughout time remains incomplete. This includes the role of ion chemistry in liberating H from water and in driving nonthermal escape, and the degree to which the processes operating at present can be extrapolated into the past. Models of H production from water via ion chemistry in the upper atmosphere by Fox (2015), Krasnopolsky (2019), and Stone et al. (2020) suggest that ion chemistry may be significant in liberating H from water, but the relative importance of this process has been shown to be subdued by direct photolysis (Montmessin et al. 2022). In addition, reactions involving H-bearing ions are expected to produce nonthermal hydrogen atoms, which may contribute a significant component of H loss (Gregory et al. 2023; Cangi et al. 2023). Similar hot hydrogen production mechanisms may result in a substantial nonthermal component, which may be required to explain some observations of upper atmospheric H (Chaufray et al. 2008; Bhattacharyya et al. 2015; Chaffin et al. 2018). In addition, the role of solar activity in controlling H loss is not well understood, despite hints that higher solar input can increase loss rates on short timescales (Mayyasi et al. 2017). Finally, the thermal and non-thermal loss processes operating at present are dependent on the details of the present-day climate and water seasonal cycle. Both are likely to be very different at other times in Mars history as a result of obliquity and eccentricity variations. It is not known if the present-day processes are dominant over Mars history, or how to best extrapolate them to infer long-term average H loss rates.

8 A Tale of Isotopes: HDO in the Martian Atmosphere

One avenue for understanding the long-term loss of H to space is the enriched isotope ratio in atmospheric water (HDO/H_2O), which records the integrated effect of differential escape of H and D on the exchangeable water reservoir. While MEx made a considerable contribution to H escape, it was not equipped to identify D or HDO. However, both D and HDO have been subsequently measured by MAVEN (D) and TGO (HDO), making MEX, MAVEN, and TGO pivotal for understanding the fate of Mars' water and its isotopologues. This section is intended to shed a light on this important topic for which MEx paved the way, despite not measuring water and hydrogen isotopes.

8.1 What We Know from Ground-Based Observations

HDO on Mars was first identified using ground-based high-resolution spectra in the NIR range (Owen et al. 1988). A D/H value of $6 \pm 3 \times$ VSMOW was inferred, supporting the idea of an early escape of hydrogen in the history of Mars and a warmer and wetter ancient atmosphere. Subsequent ground-based measurements were obtained (Novak et al. 2011; Krasnopolsky 2015; Villanueva et al. 2015), with first maps of D/H obtained for different seasons from spring equinox to northern summer solstice using several ground-based observatories at mid-infrared wavelengths (Villanueva et al. 2015). In the TIR, maps obtained with the EXES imaging spectrometer aboard SOFIA (Stratospheric Observatory for Infrared Astronomy), revealed less spatial variability but were in global agreement with previous ground-based measurements (Encrenaz et al. 2016, 2018). These column measurements revealed a common general trend, in which the D/H fractionation is primarily driven by condensation/sublimation effects. The HDO/H_2O in the gas phase increases as a function of increasing temperature and lower available condensation nuclei, leading to hemispheric and localized D/H enhancements (Villanueva et al. 2015; Encrenaz et al. 2016) .

8.2 Theory vs. Observations

As water is released from the Mars surface, cycled through the atmosphere/clouds/surface with a small fraction escaping to space, not all the water isotopes go through this cycling and escape processes in the same way. For instance, HDO has a different condensation temperature (CIFE: Condensation Induced Fractionation Effect), a different photolysis rate (PIFE: Photolysis Induced Fractionation Effect), and the escape rates for D and H are notably different considering the factor of two difference in mass between the atomic isotopes. Therefore, measurements of isotopic ratios, and in particular D/H in water, provide a powerful method to constrain volatile escape and to track the transport of water between reservoirs (e.g., seasonal transport between the polar caps). Because the escape rates for each isotope are different, over long periods, the atmosphere becomes enriched in the heavy isotopic forms. Importantly, by mapping the current isotopic ratios, one can also test for the existence of different volatile reservoirs (e.g., polar caps, regolith) with distinct isotopic signatures.

An updated picture of these processes on Mars is now available thanks to ExoMars/TGO (Trace Gas Orbiter), which provides simultaneous observations of H_2O, D/H and water ice up to 65 km (Fig. 15). For instance, TGO/NOMAD observations have shown that in the lower atmosphere the main factor controlling the D/H vertical variability is Rayleigh distillation and condensation into water ice, as HDO drops dramatically right above the top of water ice clouds (Alday et al. 2021; Villanueva et al. 2021, 2022). These observations also reveal that the vertical distribution of water ice shows little interannual variation, once the effects of occasional global-scale events such as the 2018 GDS are taken out.

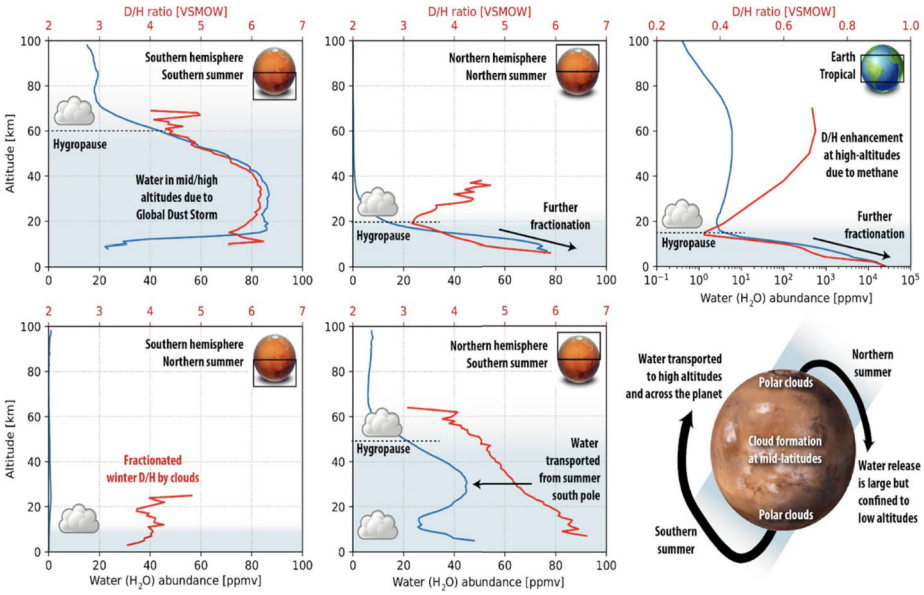

Fig. 15 Average water (blue trace) and D/H (red trace) profiles during local summer (upper-panels) and local-winter (lower-panels) as measured with TGO/NOMAD (Villanueva et al. 2022). Southern summer is L_S 240-290 MY34, northern summer is LS 70-120 MY35. Fractionation across the atmosphere is relatively strong, with the D/H being highly affected by the local climate. Therefore, these average profiles are primarily relevant when exploring general vertical morphologies, not for extracting absolute values. During southern summer and the GDS, water is brought to high-altitudes, and it is also transported effectively to the winter hemisphere. During northern summer, the hygropause is quite compact and the D/H shows a strong fractionation with altitude, similar to what occurs on our planet. Reproduced with permission from Villanueva et al. (2022), copyright by AGU

Importantly, TGO data have clarified the role of water ice clouds in the water cycle and D/H, providing the direct connections between cloud microphysics, radiative effects and cloud formation processes and the D/H variability (Aoki et al. 2019; Fedorova et al. 2020; Liuzzi et al. 2020; Villanueva et al. 2021, 2022). NOMAD observations have preliminarily shown that ice particle sizes at 30-50 km are anti-correlated to water vapor availability during dust events (Liuzzi et al. 2020), possibly having an effect on condensation-induced fractionation. At perihelion, the maximum altitude at which water ice forms is usually close to 90 km in both hemispheres, while at aphelion this decreases to ∼50 km at the equator, while water ice presence is very elusive at southern latitudes. Observations of water ice clouds at high latitudes reveal a compressed hygropause in the aphelion season, which makes the vertical transport of water much more limited than in the southern summer, resulting in lower-altitude clouds and steep vertical variations of the D/H (Villanueva et al. 2022).

8.3 HDO Fractionation: A View from Theory

Atmospheric models that include CIFE, predicted some of this D/H variability, with HDO sequestration in the lower atmosphere (<40 km) as a consequence of water ice formation around the hygropause and further transfer of HDO enriched icy particles below the cloud base where they evaporate and release gaseous H_2O enriched with HDO (Fouchet and Lellouch 2000; Bertaux and Montmessin 2001). This effect was then represented and confirmed

with 3D HDO cycle model embedded in Mars Global Climate Models (Daerden et al. 2022; Montmessin et al. 2005). However, these 3D models also show that CIFE not only operates on the vertical distribution of HDO relative to H_2O, but also on its horizontal distribution: In the two polar regions during fall and winter, the cold atmosphere leads to large-scale water condensation and becomes severely depleted in HDO (as confirmed by observations and reported in Villanueva et al. 2022), creating a twofold depletion of the HDO column relative to that of H_2O. Recent modeling work (Vals et al. 2022) improved the 3D HDO condensation scheme to include the effects of microphysics. In particular, the lower diffusivity of HDO than H_2O while condensing (i.e., kinetic effect) can counterbalance the preferential condensation of HDO due to their differences in vapor pressure (Jouzel and Merlivat 1984). This kinetic effect, increasingly important in the presence of supersaturation, effectively softens the variations of D/H in the atmosphere of Mars caused by CIFE (Vals et al. 2022). Similarly, surface-atmosphere exchange via adsorption on the regolith has also been speculated to produce substantial variations in the HDO/H_2O near-surface ratio (Hu 2019) due to their differences in their adsorption energy. This fractionation effect is expected to produce a characteristic diurnal cycle in the D/H ratio within the planetary boundary layer following variations in the surface temperature, with higher values of D/H during the day than the night.

Beyond condensation effects (CIFE), another fractionation effect introduced by photolysis (PIFE) has been predicted to influence the fate of HDO and D/H. The reduced UV cross-sections of HDO relative to its main isotope (Cheng et al. 1999) makes HDO less efficiently destroyed through photolysis than H_2O by a factor of 2-3 in the lower atmosphere. The effect of this process in the isotope composition of water is most noticeable in the middle and upper atmospheres, where photolysis is most effective. Photolysis is predicted to increase the values of the D/H ratio in water by approximately 20% at 80 km (Vals et al. 2022). While water is the major reservoir of hydrogen on Mars, its escape to space does not occur in the form of water vapor but in the form of lighter species such as atomic and molecular hydrogen and their deuterated analogues. Therefore, the first part of the water escape mechanism comprises the production of these species and the corresponding fractionation of D/H. Shortly after the measurement of depleted D/H in molecular hydrogen in the upper atmosphere (Krasnopolsky et al. 1998), both CIFE and PIFE were suggested as plausible mechanisms for explaining such isotopic fractionation, and it has long remained unclear which of the two effects dominates. Recent observations from the ExoMars TGO (Alday et al. 2021; Villanueva et al. 2022) together with modeling work including both fractionation types (Vals et al. 2022) show PIFE to have the highest importance around perihelion, making it a key effect in the relative escape of water isotopes on Mars. This is because the perihelion season hosts a combination of processes that throttles atmospheric condensation and leads the atmosphere to be highly supersaturated in water vapor at an altitude ($>$60 km) where photolysis becomes prevalent in the H and D production (Chaffin et al. 2017; Aoki et al. 2019; Fedorova et al. 2020, 2023; Montmessin et al. 2022).

8.4 Deuterium and Hydrogen: A Key to Elucidate Water Escape?

Interpretation of this observed 5-6$\times$ enhancement relative to Earth requires knowledge of the size of the present-day exchangeable reservoir and knowledge of the fractionation factor of H and D escape to space. This factor was estimated by Yung et al. (1988) as 0.32 based on early high thermosphere temperatures inferred by Mariner 6 and 7 (Anderson and Hord 1971). Later estimates of the fractionation factor by Krasnopolsky (2002), Cangi et al. (2020), and Cangi et al. (2023) give much lower values, consistent with almost complete

D retention by the planet. Based on the available data, it is clear that present-day H loss rates are insufficient to remove the amount of water lost, as inferred from estimates of the contemporary water loss rate. Resolution of this discrepancy will likely require a detailed understanding of the loss process operating today so that they can be more reliably extrapolated to the geologically recent past.

9 Conclusion

Mars Express has been able to characterize water in nearly all its forms, on the ground and in the air, supplying key constraints to challenge model predictions and help improve them (see for instance Navarro et al. 2014). With its multiple instruments capable of measuring column abundances of water vapor, MEx has allowed reappraising the knowledge gained by previous missions, in particular by leading to revisit previous reference datasets that suffered from some, as of then, unidentified flaws. Imaging water vapor at the surface was one of the unique contributions of MEx as it could rely on the hyperspectral imaging capability of OMEGA to track the instantaneous water vapor horizontal distribution near the northern pole and away from it. Coupled to surface frost survey (again by OMEGA), it has been possible to consider Mars' water cycle through the angle of the behavior of its two main components. In doing so, MEx contributed to the long and dense exploration of Mars' water cycle that was initiated and further pursued by several NASA missions (Mariner's, Viking, MGS, MRO) and also paved the way to TGO.

One of the most important contributions of MEx concerns the seasonal and latitudinal variations of the water column abundance, which has been monitored for the first time by more than one instrument on the same spacecraft. The cross-comparison work that this enabled has led to a better understanding of the main problems affecting water vapor retrievals. The multi-year study conducted by MEx covered years with and without dust storms, enabling us to understand how increased dust could disrupt the water cycle and/or retrievals.

MEx has enabled extensive monitoring of the variation in seasonal deposits of CO_2 and H_2O ice, thanks to the diagnostic signatures of this ice in the near and mid-infrared. This study has enabled us to better characterize the retreat of the northern polar ice cap, by highlighting a sublimation-recondensation cycle controlled by very active surface-atmosphere water exchanges, which 3D models had been predicting for long.

The vertical distribution of water could also be addressed in an unprecedented way thanks to the use, for the first time around Mars, of solar occultation by SPICAM that has allowed profiling water vapor at various places and seasons regularly for two decades. This led to a number of findings; in particular, the unexpected occurrence of large amounts of supersaturation, as well as the drastic changes in the water vapor profiles between aphelion and perihelion. All of these findings have been now explored in more depth and documented far more extensively by TGO and its two IR spectrometers (NOMAD and ACS), both operating in solar occultation as well.

MEx also experimented an original way to probe the vertical distribution of water from an observing geometry, nadir, that has long been considered to be limited to the column abundance of water vapor. Combining SPICAM and PFS in a synergistic way enabled exploring the water confinement in the lowest 5 km relative to the rest of the column. This kind of synergy, derived from a technique employed with Earth orbiters, could inspire the design of future instruments.

Finally, MEx also allowed establishing a direct link that was not anticipated between the lower atmospheric water and its atomic by-products in the exosphere, among which H

atoms are the most regarded for they can escape Mars' gravity and deplete Mars of its primordial water. This "highway to space", evidenced by the concomitant solar occultation and Lyman-α observations, has led to a major paradigm shift consisting in the unexpected rapid transfer of water at high altitude around perihelion, and leading to seasonal variations in the exospheric hydrogen population. This finding has been further consolidated by MAVEN, which can measure H and D and showed comparable seasonal variations for these two atoms, and by TGO whose extreme sensitivity has been able to document the concomitant transfer of water vapor up to 120 km of altitude. The ramifications of this discovery are still incompletely appreciated, yet have already shed a new light on water escape in the long term.

Added to TGO's, MAVEN's, and other NASA missions; MEx's harvest has placed the community at the eve of a revolution for our understanding of the fate of water on Mars.

Declarations

Competing Interests The authors declare that there are no conflicts of interest or competing interests.

References

Alday J, Trokhimovskiy A, Irwin PGJ, Wilson CF, Montmessin F, Lefévre F, et al (2021) Isotopic fractionation of water and its photolytic products in the atmosphere of Mars. Nat Astron 5(9):943–950. https://doi.org/10.1038/s41550-021-01389-x

Anderson DE (1974) Mariner 6, 7 and 9 ultraviolet spectrometer experiment: analysis of hydrogen Lyman-α data. J Geophys Res. https://doi.org/10.1029/JA079i010p01513

Anderson DE, Hord CW (1971) Mariner 6 and 7 ultraviolet spectrometer experiment: analysis of hydrogen Lyman-α data. J Geophys Res. https://doi.org/10.1029/JA076i028p06666

Aoki S, Vandaele AC, Daerden F, Villanueva GL, Liuzzi G, Thomas IR, et al (2019) Water vapor vertical profiles on Mars in dust storms observed by TGO/NOMAD. J Geophys Res, Planets 124(12):3482–3497. https://doi.org/10.1029/2019JE006109

Aoki S, Vandaele AC, Daerden F, Villanueva GL, Liuzzi G, Clancy RT, et al (2022) Global vertical distribution of water vapor on Mars: results from 3.5 years of ExoMars-TGO/NOMAD science operations. J Geophys Res, Planets 127(9):e2022JE007231. https://doi.org/10.1029/2022JE007231

Appéré T, Schmitt B, Langevin Y, Douté S, Pommerol A, Forget F, Spiga A, Gondet B, Bibring JP (2011) Winter and spring evolution of northern seasonal deposits on Mars from OMEGA on Mars Express. J Geophys Res, Planets 116(E5):E05001. https://doi.org/10.1029/2010JE003762

Audouard J, Poulet F, Vincendon M, Milliken RE, Jouglet D, Bibring JP, Gondet B, Langevin Y (2014) Water in the Martian regolith from OMEGA/Mars Express. J Geophys Res, Planets 119(8):1969–1989. https://doi.org/10.1002/2014JE004649

Barth CA, et al (1969) Mariner 6: ultraviolet spectrum of Mars upper atmosphere. Science 165:1004–1005. https://doi.org/10.1126/Science.165.3897.1004

Barth CA, Stewart AI, Hord CW, Lane AL (1972) Mariner 9 ultraviolet spectrometer experiment: Mars airglow spectroscopy and variations in Lyman alpha. Icarus 17:457–468. https://doi.org/10.1016/0019-1035(72)90011-5

Belyaev DA, et al (2021) Revealing a high water abundance in the upper mesosphere of Mars with ACS onboard TGO. Geophys Res Lett 48(10):e2021GL093411. https://doi.org/10.1029/2021GL093411

Bertaux JL, et al (1995) SWAN: a study of the solar wind anisotropies on SOHO with Lyman-α sky mapping. Sol Phys 162:403–439. https://doi.org/10.1007/BF00733435

Bertaux JL, and Montmessin F (2001) Isotopic fractionation through water vapor condensation: The Deuteropause, a cold trap for deuterium in the atmosphere of Marss. J Geophys Res, Planets 106(12), p. 32879-32884 https://doi.org/10.1029/2006JE002690

Bertaux JL, Leblanc F, Perrier S, Quemerais E, Korablev O, Dimarellis E, Reberac A, Forget F, Simon PC, Stern SA, Sandel B (2005) Nightglow in the Upper Atmosphere of Mars and Implications for Atmospheric Transport. Science 307(2709):566–569. https://doi.org/10.1126/science.1106957

Bertaux JL, et al (2006) SPICAM on Mars Express: Observing modes and overview of UV spectrometer data and scientific results. J Geophys Res, Planets 111(10). https://doi.org/10.1029/2006JE002690

Bhattacharyya D, Clarke J, Bertaux JL, Chaufray JY, Mayyasi M (2015) A strong seasonal dependence in the Martian hydrogen exosphere. Geophys Res Lett 42(20):8678–8685. https://doi.org/10.1002/2015gl065804

Bhattacharyya D, Clarke J, Bertaux JL, Chaufray JY, Mayyasi M (2017) Analysis and modeling of remote observations of the Martian hydrogen exosphere. Icarus 281:264–280. https://doi.org/10.1016/j.icarus.2016.08.034

Bhattacharyya D, Chaufray JY, Mayyasi M, Clarke JT, Stone S, Yelle RV, et al (2020) Two-dimensional model for the Martian exosphere: applications to hydrogen and deuterium Lyman α observations. Icarus 339:113573. https://doi.org/10.1016/j.icarus.2019.113573

Bibring J, et al (2004) Perennial water ice identified in the south polar cap of Mars. Nature 428:627–630. https://doi.org/10.1038/nature02461

Böttger HM, Lewis SR, Read PL, Forget F (2005) The effects of the Martian regolith on GCM water cycle simulations. Icarus 177:174–189. https://doi.org/10.1016/j.icarus.2005.02.024

Brines A, et al (2023) Water vapor vertical distribution on Mars during perihelion season of MY 34 and MY 35 with ExoMars-TGO/NOMAD observations. J Geophys Res, Planets e2022JE007273. https://doi.org/10.1029/2022JE007273

Cangi EM, Chaffin MS, Deighan J (2020) Higher Martian atmospheric temperatures at all altitudes increase the D/H fractionation factor and water loss. J Geophys Res, Planets 125(12):e06626. https://doi.org/10.1029/2020JE006626

Cangi EM, Chaffin MS, Yelle R, Gregory B, Deighan J (2023) Fully coupled photochemistry of the deuterated ionosphere of Mars and its effects on escape of H and D. J Geophys Res, Planets 128(7):e2022JE007713. https://doi.org/10.1029/2022JE007713

Carr MH (1987) Water on Mars. Nature 326:30–35. https://doi.org/10.1038/326030a0.

Chaffin MS, Chaufray JY, Stewart AI, Montmessin F, Schneider NM, Bertaux JL (2014) Unexpected variability of Martian hydrogen escape. Geophys Res Lett 41(2):314–320. https://doi.org/10.1002/2013gl058578

Chaffin MS, Deighan J, Schneider NM, Stewart AI (2017) Elevated atmospheric escape of atomic hydrogen from Mars induced by high-altitude water. Nat Geosci 10(3):174–178. https://doi.org/10.1038/ngeo2887

Chaffin MS, et al (2018) Mars H escape rates derived from MAVEN/IUVS Lyman alpha brightness measurements and their dependence on model assumptions. J Geophys Res, Planets 123(8):2192–2210. https://doi.org/10.1029/2018JE005574

Chaffin MS, et al (2021) Martian water loss to space enhanced by regional dust storms. Nat Astron 5:1036–1042. https://doi.org/10.1038/s41550-021-01425-w

Chaufray JY, Bertaux JL, Leblanc F, Quémerais E (2008) Observation of the hydrogen corona with SPICAM on Mars Express. Icarus 195:598–613. https://doi.org/10.1016/j.icarus.2008.01.009

Chaufray JY, et al (2021a) Study of the hydrogen escape rate at Mars during Martian years 28 and 29 from comparisons between SPICAM/Mars Express and GCM-LMD simulations. Icarus 353. https://doi.org/10.1016/j.icarus.2019.113498

Chaufray JY, et al (2021b) Estimate of the D/H ratio in the Martian upper atmosphere from the low spectral resolution mode of MAVEN/IUVS. J Geophys Res, Planets 126(4):e06814. https://doi.org/10.1029/2020JE006814

Cheng DA, et al (1999) Photo-induced fractionation of water isotopomers in the Martian atmosphere. Geophys Res Lett 26(24):3657–3660. https://doi.org/10.1029/1999GL008367

Clancy RT, et al (1996) Water vapor saturation at low altitudes around Mars Aphelion: a key to Mars climate? Icarus 122:36–62. https://doi.org/10.1006/icar.1996.0108

Clarke JT, et al (2014) A rapid decrease of the hydrogen corona of Mars. Geophys Res Lett 41:8013–8020. https://doi.org/10.1002/2014GL061803

Clarke JT, et al (2017) Variability of d and h in the Martian upper atmosphere observed with the maven IUVS echelle channel. J Geophys Res Space Phys 122:2336–2344. https://doi.org/10.1002/2016JA023479

Clarke JT, et al (2024) Martian atmospheric hydrogen and deuterium: Seasonal changes and paradigm for escape to space. Science Advances 10:eadm7499. https://doi.org/10.1126/sciadv.adm7499

Conrath B, et al (1973) Atmospheric and surface properties of Mars obtained by infrared spectroscopy on Mariner 9. J Geophys Res 78(20):4267–4278. https://doi.org/10.1029/JB078i020p04267

Daerden F, Neary L, Villanueva G, Liuzzi G, Aoki S, Clancy RT, et al (2022) Explaining NOMAD D/H Observations by Cloud-Induced Fractionation of Water Vapor on Mars. J Geophys Res, Planets 127(2). https://doi.org/10.1029/2021JE007079

Encrenaz T, et al (2005) A mapping of Martian water sublimation during early northern summer using OMEGA/Mars Express. Astron Astrophys 441:L9–L12. https://doi.org/10.1051/0004-6361:200500171.

Encrenaz T, et al (2008) A study of the Martian water vapor over Hellas using OMEGA and PFS aboard Mars Express. Astron Astrophys 484:547–553. https://doi.org/10.1051/0004-6361:20079288

Encrenaz T, et al (2016) A map of D/H on Mars in the thermal infrared using EXES aboard SOFIA. Astron Astrophys 586:id.A62, 12 pp. https://doi.org/10.1051/0004-6361/20152701

Encrenaz T, et al (2018) New measurements of D/H on Mars using EXES aboard SOFIA. Astron Astrophys 612:id.A112, 13 pp. https://doi.org/10.1051/0004-6361/201732367

Fedorova A, Rodin AV, Baklanova IV (2004) MAWD observations revisited: seasonal behavior of water vapor in the martian atmosphere Icarus 171(1):54–67. https://doi.org/10.1016/j.icarus.2004.04.017

Fedorova A, Korablev O, Bertaux JL, Rodin A, Kiselev A, Perrier S (2006) J Geophys Res, Planets Mars water vapor abundance from SPICAM IR spectrometer: Seasonal geographic distributions. 111(9). https://doi.org/10.1029/2006JE002695

Fedorova AA, Korablev OI, Bertaux J-L, Rodin AV, Montmessin F, Belyaev DA, Reberac A (2009) Solar infrared occultation observations by SPICAM experiment on Mars-Express: simultaneous measurements of the vertical distributions of H_2O, CO_2 and aerosol. Icarus 200(1):96–117. https://doi.org/10.1016/j.icarus.2008.11.006

Fedorova A, Trokhimovsky A, Korablev O, Montmessin F (2010) Viking observation of water vapor on Mars: revision from up-to-date spectroscopy and atmospheric models. Icarus 208:156–164. https://doi.org/10.1016/j.icarus.2010.01.018

Fedorova A, Montmessin F, Rodin AV, Korablev OI, Määttänen A, Maltagliati L, Bertaux JL (2014) Evidence for a bimodal size distribution for the suspended aerosol particles on Mars. Icarus 231:239–260. https://doi.org/10.1016/j.icarus.2013.12.015

Fedorova A, Bertaux JL, Betsis D, Montmessin F, Korablev O, Maltagliati L, Clarke J (2018) Water vapor in the middle atmosphere of Mars during the 2007 global dust storm. Icarus 300:440–457. https://doi.org/10.1016/j.icarus.2017.09.025

Fedorova A, Montmessin F, Korablev O, et al (2020) Stormy water on Mars: the distribution and saturation of atmospheric water during the dusty season. Science 367:297–300. https://doi.org/10.1126/science.aay9522

Fedorova A, Montmessin F, Korablev O, Lefèvre F, Trokhimovskiy AV, Bertaux JL (2021) Multi-Annual Monitoring of the Water Vapor Vertical Distribution on Mars by SPICAM on Mars Express. J Geophys Res, Planets 126. https://doi.org/10.1029/2020JE006616

Fedorova A, et al (2023) A two-Martian years survey of the water vapor saturation state on Mars based on ACS NIR/TGO occultations. J Geophys Res, Planets 128(1):e2022JE007348. https://doi.org/10.1029/2022JE007348

Fischer E, Martínez GM, Rennó NO, Tamppari LK, Zent AP (2019) Relative humidity on Mars: new results from the Phoenix TECP sensor. J Geophys Res, Planets 124(11):2780–2792

Formisano V, et al (2005) The Planetary Fourier Spectrometer (PFS) onboard the European Mars Express mission. Planet Space Sci 53:963. https://doi.org/10.1016/j.pss.2004.12.006

Fouchet T, Lellouch E (2000) Vapor pressure isotope fractionation effects in planetary atmospheres: application to deuterium. Icarus 144(1):114–123. https://doi.org/10.1006/icar.1999.6264

Fouchet T, et al (2007) Martian water vapor: Mars Express PFS/LW observations. Icarus 190(1):32–49. https://doi.org/10.1016/j.icarus.2007.03.003

Fox JL (2015) The chemistry of protonated species in the Martian ionosphere. Icarus 252:366–392. https://doi.org/10.1016/j.icarus.2015.01.010

Gregory BS, Elliott RD, Deighan J, Gröller H, Chaffin MS (2023) HCO^+ dissociative recombination: a significant driver of nonthermal hydrogen loss at Mars. J Geophys Res, Planets 128(1):e2022JE007576. https://doi.org/10.1029/2022JE007576

Halekas JS (2017) Seasonal variability of the hydrogen exosphere of Mars. J Geophys Res, Planets 122:901–911. https://doi.org/10.1002/2017JE005306

Heavens NG, et al (2018) Hydrogen escape from Mars enhanced by deep convection in dust storms. Nat Astron 2(2):126–132. https://doi.org/10.1038/s41550-017-0353-4

Holmes JA, et al (2021) Enhanced water loss from the Martian atmosphere during a regional-scale dust storm and implications for long-term water loss. Earth Planet Sci Lett 571:117109. https://doi.org/10.1029/2022JE007203

Holmes JA, et al (2022) Global variations in water vapor and saturation state throughout theMmars year 34 dusty season. J Geophys Res, Planets 127(10):e2022JE007203

Hord C, Barth C, Pearce J (1970) Ultraviolet spectroscopy experiment for Mariner Mars 1971. Icarus 12(1):63–77. https://doi.org/10.1016/0019-1035(70)90032-1

Houben H, Haberle RM, Young RE, Zent AP (1997) Modeling the Martian seasonal water cycle. J Geophys Res, Planets 102(E4):9069–9083. https://doi.org/10.1029/97JE00046

Hu R (2019) Predicted diurnal variation of the deuterium to hydrogen ratio in water at the surface of Mars caused by mass exchange with the regolith. Earth and Plan Science Lett 519:192–201. https://doi.org/10.1016/j.epsl.2019.05.017

Hunten DM (1973) The escape of light gases from planetary atmospheres. J Atmos Sci 30:1481–1494. https://doi.org/10.1175/1520-0469(1973)030<1481:TEOLGF>2.0.CO;2

Jakosky BM, Farmer CB (1982) The seasonal and global behavior of water vapor in the Mars atmosphere — complete global results of the Viking atmospheric water detector experiment. J Geophys Res, Planets 87:2999–3019. https://doi.org/10.1029/JB087iB04p02999

Jakosky BM, Lin RP, Grebowsky JM, Luhmann JG, Mitchell DF, Beutelschies G, et al (2015) The Mars atmosphere and volatile evolution (MAVEN) mission. Space Sci Rev 195(1–4):3–48. https://doi.org/10.1007/s11214-015-0139-x

Jakosky BM (2021) Atmospheric loss to space and the history of water on Mars. Annu Rev Earth Planet Sci 49(1):71–93. https://doi.org/10.1146/annurev-earth-062420-052845

Jouzel J, Merlivat L (1984) Deuterium and oxygen 18 in precipitation: modeling of the isotopic effects during snow formation. J Geophys Res 89(D7):11749. https://doi.org/10.1029/JD089iD07p11749

Kahre MA, Haberle RM, Hollingsworth JL, Wolff MJ (2020) MARCI-observed clouds in the hellas basin during northern hemisphere summer on Mars: interpretation with the NASA/Ames legacy Mars global climate model. Icarus 338:113512. https://doi.org/10.1016/j.icarus.2019.113512

Kleinböhl A, Schofield JT, Kass DM, Abdou WA, Backus CR, Sen B, et al (2009) Mars Climate Sounder limb profile retrieval of atmospheric temperature, pressure, and dust and water ice opacity. J Geophys Res, Planets 114(E10):2009JE003358. https://doi.org/10.1029/2009JE003358

Knutsen EW, Montmessin F, Verdier L, et al (2022) Water vapor on Mars: a refined climatology and constraints on the near-surface concentration enabled by synergistic retrievals. J Geophys Res, Planets 127(5):e2022JE007252. https://doi.org/10.1029/2022JE007252

Korablev O, Bertaux JL, Fedorova A, et al (2006) SPICAM IR acousto-optic spectrometer experiment on Mars Express. J Geophys Res, Planets 111:E09S03. https://doi.org/10.1029/2006JE002696

Korablev O, et al. (2006) Water in Mars atmosphere: comparison of recent data sets. Second workshop on Mars atmosphere modelling and observations, Granada

Krasnopolsky VA, Mumma MJ, Gladstone GR (1998) Detection of atomic deuterium in the upper atmosphere of Mars. Science 280(5369):1576–1580. https://doi.org/10.1126/science.280.5369

Krasnopolsky VA (2002) Mars' upper atmosphere and ionosphere at low, medium, and high solar activities: Implication for evolution of water. J Geophys Res 107(E12). https://doi.org/10.1029/2001JE001809

Krasnopolsky VA (2015) Variations of the HDO/H2O ratio in the martian atmosphere and loss of water from Mars. Icarus 257:377–386. https://doi.org/10.1016/j.icarus.2015.05.021

Krasnopolsky VA (2019) Photochemistry of water in the Martian thermosphere and its effect on hydrogen escape. Icarus 321:62–70. https://doi.org/10.1016/j.icarus.2018.10.033

Langevin Y, Poulet F, Bibring JP, Schmitt B, Douté S, Gondet B (2005) Summer evolution of the North polar cap of Mars as observed by OMEGA/Mars Express. Science 307(5715):1581–1584. https://doi.org/10.1126/science.1109438

Langevin Y, et al (2007) Observations of the south seasonal cap of Mars during recession in 2004–2006 by the OMEGA visible/near-infrared imaging spectrometer on board Mars Express. J Geophys Res, Planets 112(E8). https://doi.org/10.1029/2006JE002841

Leblanc F, Chaufray JY, Witasse O, Lilensten J, Bertaux JL (2006) The Martian dayglow as seen by SPICAM-UV spectrometer on Mars Express. J Geophys Res 111(E9). https://doi.org/10.1029/2005JE002664

Leung CW, Tamppari LK, Kass DM, Martínez G, Fischer E, Smith MD (2024) Seasonal vertical water vapor distribution at the Mars Phoenix Lander site. Icarus 408:115820

Liuzzi G, Villanueva GL, Crismani MMJ, Smith MD, Mumma MJ, Daerden F, et al (2020) Strong variability of Martian water ice clouds during dust storms revealed from ExoMars Trace Gas Orbiter/NOMAD. J Geophys Res, Planets 125(4). https://doi.org/10.1029/2019JE006250

Maltagliati L, Titov DV, Encrenaz T, Melchiorri R, Forget F, Garcia-Comas M, et al (2008) Observations of atmospheric water vapor above the Tharsis volcanoes on Mars with the OMEGA/MEx imaging spectrometer. Icarus 194(1):53–64. https://doi.org/10.1016/j.icarus.2007.09.027

Maltagliati L, Montmessin F, Fedorova A, Korablev O, Forget F, Bertaux JL (2011) Evidence of water vapor in excess of saturation in the atmosphere of Mars. Science 333(6051):1868–1871. https://doi.org/10.1126/science.1207957

Maltagliati L, Montmessin F, Korablev O, Fedorova A, Forget F, Määttänen A, Lefèvre F, Bertaux JL (2013) Annual survey of water vapor vertical distribution and water-aerosol coupling in the Martian atmosphere observed by SPICAM/MEx solar occultations. Icarus 223(2):942–962. https://doi.org/10.1016/j.icarus.2012.12.012

Maurice S, et al (2011) Mars Odyssey neutron data: 1. Data processing and models of water-equivalent-hydrogen distribution. J Geophys Res, Planets 116(E11). https://doi-org.insu.bib.cnrs.fr/10.1029/2011JE003810

Mayyasi M, Clarke J, Bhattacharyya D, Deighan J, Jain S, Chaffin M, et al (2017) The variability of atmospheric deuterium brightness at Mars: evidence for seasonal dependence. J Geophys Res Space Phys 122(10). https://doi.org/10.1002/2017JA024666

Mayyasi M, et al (2018) Significant space weather impact on the escape of hydrogen from Mars. Geophys Res Lett 45(17):8844–8852. https://doi.org/10.1029/2018GL077727

Mayyasi M, et al (2019) Seasonal variability of deuterium in the upper atmosphere of Mars. J Geophys Res Space Phys 124(3):2152–2164. https://doi.org/10.1029/2018JA026244

Mayyasi M, Clarke J, Bertaux JL, Deighan J, Bhattacharyya D, Chaffin M, et al (2023) Upgrades to the MAVEN echelle data reduction pipeline: new calibration standard and improved faint emission detection algorithm at Lyman-α. Earth Space Sci 10(4):e2022EA002602. https://doi.org/10.1029/2022EA002602

McClintock WE, Schneider NM, Holsclaw GM, Clarke JT, Hoskins AC, Stewart I, et al (2015) The Imaging Ultraviolet Spectrograph (IUVS) for the MAVEN mission. Space Sci Rev 195(1–4):75–124. https://doi.org/10.1007/s11214-014-0098-7

McElroy MB, Donahue TM (1972) Stability of the Martian atmosphere. Science 177:986–988. https://doi.org/10.1126/Science.177.4053.986

Melchiorri R, et al (2007) Water vapor mapping on Mars using OMEGA/Mars Express. Planet Space Sci 55(3):333–342. https://doi.org/10.1016/j.pss.2006.05.040

Melchiorri R, et al (2009) OMEGA/Mars Express: south pole region, water vapor daily variability. Icarus 201(1):102–112. https://doi.org/10.1016/icarus.2008.12.018

Milliken RE (2007) Hydration state of the Martian surface as seen by Mars Express OMEGA: 2. H2O content of the surface. J Geophys Res, Planets 112(E8):E08S07. https://doi.org/10.1029/2006JE002853

Millour E, et al. (2017) The Mars Climate Database (MCD version 5.3), 19th EGU General Assembly, Vienna: p.12247

Mitrofanov IG, et al (2004) Soil water content on Mars as estimated from neutron measurements by the HEND instrument onboard the 2001 Mars Odyssey spacecraft. Sol Syst Res 38(4):253–257. https://doi.org/10.1023/B:SOLS.0000037461.70809.45

Montmessin F, Ferron S (2019) A spectral synergy method to retrieve Martian water vapor column-abundance and vertical distribution applied to Mars Express SPICAM and PFS nadir measurements. Icarus 317:549–569. https://doi.org/10.1016/j.icarus.2018.07.022

Montmessin F, Forget F, Rannou P, Cabane M, Haberle RM (2004) Origin and role of water ice clouds in the Martian water cycle as inferred from a general circulation model. J Geophys Res, Planets 109(10):1–26. https://doi.org/10.1029/2004JE002284

Montmessin F, Fouchet T, Forget F (2005) Modeling the annual cycle of HDO in the Martian atmosphere. J Geophys Res, Planets 110:3006. https://doi.org/10.1029/2004JE002357

Montmessin F, Haberle RM, Forget F, Langevin Y, Clancy RT, Bibring JP (2007) On the origin of perennial water ice at the south pole of Mars: a precession-controlled mechanism? J Geophys Res, Planets 112(8). https://doi.org/10.1029/2007JE002902

Montmessin F, Smith MD, Langevin Y, Mellon MT, Fedorova A (2017a) The water cycle. In: Haberle RM, et al (eds) The atmosphere and climate of Mars. Cambridge University Press, Cambridge, pp 338–373. https://doi.org/10.1017/9781139060172.011

Montmessin F, et al (2017b) SPICAM on Mars Express: a 10 year in-depth survey of the Martian atmosphere. Icarus 297:195–216. https://doi.org/10.1016/j.icarus.2017.06.022

Montmessin F, Ferron S (2019) Reappraising the Production and Transfer of Hydrogen Atoms from the Middle to the Upper Atmosphere of Mars at Times of Elevated Water Vapor. J Geophys Res, Planets 127(5):549–569. https://doi.org/10.1016/j.icarus.2018.07.022

Montmessin F, Belyaev DA, Lefèvre F, Alday J, Vals M, Fedorova A, et al (2022) Reappraising the Production and Transfer of Hydrogen Atoms from the Middle to the Upper Atmosphere of Mars at Times of Elevated Water Vapor. J Geophys Res, Planets 127(5). https://doi.org/10.1029/2022JE007217

Navarro T, Madeleine JB, Forget F, Spiga A, Millour E, Montmessin F, Määttänen A (2014) Global climate modeling of the Martian water cycle with improved microphysics and radiatively active water ice clouds. J Geophys Res, Planets 119(7):1479–1495. https://doi.org/10.1002/2013JE004550

Neary L, et al (2020) Explanation for the increase in high-altitude water on Mars observed by NOMAD during the 2018 global dust storm. Geophys Res Lett 47(7):e84354. https://doi.org/10.1029/2019GL084354

Novak RE, Mumma MJ, Villanueva GL (2011) Measurement of the isotopic signatures of water on Mars; Implications for studying methane. Plan. Space Sci 59(2-3):163–168. https://doi.org/10.1016/j.pss.2010.06.017

Owen T, Maillard JP, de Bergh C, Lutz BL (1988) Deuterium on Mars - the abundance of HDO and the value of D/H. Science 240:1767–1770. https://doi.org/10.1126/Science.240.4860.1767

Pankine AA (2022) Martian atmospheric water vapor abundances in MY26-30 from Mars Express PFS/LW observations. Icarus 379:114975. https://doi.org/10.1016/j.icarus.2022.114975

Pankine AA, Tamppari LK (2019) MGS TES observations of the water vapor in the Martian southern polar atmosphere during spring and summer. Icarus 331:26–48. https://doi.org/10.1016/j.icarus.2019.05.010

Pankine AA, Tamppari LK, Smith MD (2010) MGS TES observations of the water vapor above the seasonal and perennial ice caps during northern spring and summer. Icarus 210(1):58–71. https://doi.org/10.1016/j.icarus.2010.06.043

Pankine AA, Leung C, Leslie LK, Martinez G, Giuranna M, Piqueux S, Smith MD, Trokhimovskiy AV (2023) Effects of Global Dust Storms on Water Vapor in the Southern Polar Region of Mars. J Geophys Res, Planets 128(12). https://doi.org/10.1029/2023JE008016

Parkinson TD, Hunten DM (1972) Spectroscopy and Aeronomy of O2 on Mars. J Atmos Sci 29:1380–1390. https://doi.org/10.1175/1520-0469(1972)029<1380:SAAOOO>2.0.CO;2

Picardi G, et al (2005) Radar soundings of the subsurface of Mars. Science 310(5756):1925–1928. https://doi.org/10.1126/science.1122165

Piqueux S, Kleinböhl A, Hayne PO, Kass DM, Schofield JT, McCleese DJ (2015) Variability of the Martian seasonal CO2 cap extent over eight Mars years. Icarus 251:164–180. https://doi.org/10.1016/j.icarus.2014.10.045

Plaut JJ, et al (2007) Subsurface radar sounding of the south polar layered deposits of Mars. Science 316(5821):92–95. https://doi.org/10.1126/science.1139672

Polkko J, Hieta M, Harri AM, Tamppari L, Martínez G, Viúdez-Moreiras D, Savijärvi H, Conrad P, Zorzano Mier MP, De La Torre Juarez M, Hueso R (2023) Initial results of the relative humidity observations by MEDA instrument onboard the Mars 2020 perseverance rover. J Geophys Res, Planets 128(2):e2022JE007447

Qin J (2021) Solar cycle, seasonal, and dust-storm-driven variations of the Mars upper atmospheric state and H escape rate derived from the Ly-α emission observed by NASA's MAVEN mission. Astrophys J 912(1):77. https://doi.org/10.3847/1538-4357/abed4f

Quémerais E, Sandel BR, Izmodenov VV, Gladstone GR (2013) Thirty years of interplanetary background data: a global view. In: Quémerais E, et al (eds) Cross-calibration of far UV spectra of Solar System objects and the heliosphere. Springer, New York, pp 141–162. https://doi.org/10.1007/978-1-4614-6384-9_4

Rahmati AL, et al (2017) Maven measured oxygen and hydrogen pickup ions: probing the Martian exosphere and neutral escape. J Geophys Res Space Phys 122:3689–3706. https://doi.org/10.1002/2016JA023371

Richardson MI, Wilson RJ (2002a) Investigation of the nature and stability of the Martian seasonal water cycle with a general circulation model. J Geophys Res, Planets 107(E5):5031. https://doi.org/10.1029/2001JE001536

Richardson MI, Wilson RJ (2002b) A topographically forced asymmetry in the Martian circulation and climate. Nature 416(6878):298–301. https://doi.org/10.1038/416298a

Rodin AV, Korablev O, Moroz V (1997) Vertical distribution of water in the near-equatorial troposphere of Mars: water vapor and clouds. Icarus 125(1):212–229. https://doi.org/10.1006/icar.1996.5602

Savijärvi HI, Harri AM (2021) Water vapor adsorption on Mars. Icarus 357:114270. https://doi.org/10.1016/j.icarus.2020.114270

Savijärvi H, Harri AM, Kemppinen O (2016) The diurnal water cycle at Curiosity: role of exchange with the regolith. Icarus 265:63–69. https://doi.org/10.1016/j.icarus.2015.10.008

Selvans MM, Plaut JJ, Aharonson O, Safaeinili A (2010) Internal structure of Planum Boreum, from Mars advanced radar for subsurface and ionospheric sounding data. J Geophys Res, Planets 115:9003. https://doi.org/10.1029/2009JE003537

Shaposhnikov DS, Medvedev AS, Rodin AV, Hartogh P (2019) Seasonal water "pump" in the atmosphere of Mars: vertical transport to the thermosphere. Geophys Res Lett 46(8):4161–4169. https://doi.org/10.1029/2019GL082839

Smith MD (2002) The annual cycle of water vapor on Mars as observed by the Thermal Emission Spectrometer. J Geophys Res, Planets 107(E11). https://doi.org/10.1029/2001JE001522

Smith MD (2004) Interannual variability in TES atmospheric observations of Mars during 1999-2003. Icarus 167:148–165. https://doi.org/10.1016/j.icarus.2003.09.010

Smith MD (2009) THEMIS observations of Mars aerosol optical depth from 2002-2008. J of Geophys Res, Planets 202(2):444–452. https://doi.org/10.1016/j.icarus.2009.03.027
Smith MD, Daerden F, Neary L, Khayat A (2018) The climatology of carbon monoxide and water vapor on Mars as observed by CRISM and modeled by the GEM-Mars general circulation model. Icarus 301:117. https://doi.org/10.1016/j.icarus.2017.09.027
Spinrad H, Münch G, Kaplan LD (1963) Letter to the editor: the detection of water vapor on Mars. Astrophys J 137:1319. https://doi.org/10.1086/147613
Steele LJ, Balme MR, Lewis SR, Spiga A (2017) The water cycle and regolith–atmosphere interaction at Gale crater, Mars. Icarus 289:56–79. https://doi.org/10.1016/j.icarus.2017.02.010
Stone SW, et al (2020) Hydrogen escape from Mars is driven by seasonal and dust storm transport of water. Science 370(6518):824–831. https://doi.org/10.1126/science.aba5229
Tamppari LK, Lemmon MT (2020) Near-surface atmospheric water vapor enhancement at the Mars Phoenix lander site. Icarus 343:113624
Thomas GE (1963) Lyman-α scattering in the Earth's hydrogen corona. J Geophys Res, Planets 68:2639–2660. https://doi.org/10.1029/JZ068i009p02639
Titus TN, Kieffer HH, Christensen PR (2003) Exposed water ice discovered near the south pole of Mars. Science 299:1048–1051. https://doi.org/10.1126/science.1080497
Trokhimovskiy A, et al (2015) Mars' water vapor mapping by the SPICAM IR spectrometer: five Martian years of observations. Icarus 251:50–56. https://doi.org/10.1016/j.icarus.2014.10.007
Tschimmel M, et al (2008) Investigation of water vapor on Mars with PFS/SW of Mars Express. Icarus 195:557–575. https://doi.org/10.1016/j.icarus.2008.01.018.
Vals M, Rossi L, Montmessin F, et al (2022) Improved Modeling of Mars' HDO Cycle Using a Mars' Global Climate Model. J Geophys Res, Planets 127(8). https://doi.org/10.1029/2022JE007192
Vandaele AC, Korablev O, Daerden F, Aoki S, Thomas IR, Altieri F, et al (2019) Martian dust storm impact on atmospheric H2O and D/H observed by ExoMars Trace Gas Orbiter. Nature 568(7753):521–525. https://doi.org/10.1038/s41586-019-1097-3
Villanueva GL, et al (2015) Strong water isotopic anomalies in the martian atmosphere: Probing current and ancient reservoirs. Science 348(6231):218–221. https://doi.org/10.1126/science.aaa3630
Villanueva G, et al (2021) Water heavily fractionated with altitude on Mars as revealed by ExoMars/NOMAD. Sci Adv 7(7):eabc8843. https://doi.org/10.1126/sciadv.abc8843
Villanueva GL, et al (2022) Isotopic ratios of water released from the northern and southern caps as measured with TGO/NOMAD. Geophys Res Lett 49:e2022GL098161. https://doi.org/10.1029/2022GL098161
Whiteway JA, et al (2009) Mars water-ice clouds and precipitation. Science 325:68. https://doi.org/10.1126/science.1172344
Wilson C, et al (2024, this collection) Mars Express scientific payload and its evolution. Space Sci Rev
Yung YL, Wen JS, Pinto JP, Pierce KK, Allen M (1988) HDO in the Martian atmosphere - implications for the abundance of crustal water. Icarus 76:146–159. https://doi.org/10.1016/0019-1035(88)90147-9
Zahnle K, Haberle RM, Catling DC, Kasting JF (2008) Photochemical instability of the ancient Martian atmosphere. J Geophys Res, Planets 113(E12):11004. https://doi.org/10.1029/2008JE003160
Zent AP, Haberle RM, Houben HC, Jakosky BM (1993) A coupled subsurface-boundary layer model of water on Mars. J Geophys Res, Planets 98:3319–3337. https://doi.org/10.1029/92JE02805
Zent AP, Hecht MH, Cobos DR, Wood SE, Hudson TL, Milkovich SM, et al (2010) Initial results from the thermal and electrical conductivity probe (TECP) on Phoenix. J Geophys Res, Planets 115(E3):2009JE003420. https://doi.org/10.1029/2009JE003420